Coordinated Cross-Talk Between the Myc and Mlx Networks in Liver Regeneration and Neoplasia

Short Title: Cross-Talk Between Myc and Mlx Networks

Huabo Wang[1], Jie Lu[1], Frances Alencastro[2,3], Alexander Roberts[1], Julia Fiedor[1], Patrick Carroll[5], Robert N. Eisenman[5], Sarangarajan Ranganathan[6,] Michael Torbenson[7], Andrew W. Duncan[2,3,4] and Edward V. Prochownik[1,4,8,9,10]

[1]Division of Hematology/Oncology, UPMC Children's Hospital of Pittsburgh, Pittsburgh PA; [2]Department of Pathology, UPMC; [3]McGowan Institute for Regenerative Medicine, UPMC, Pittsburgh, PA; [4]Pittsburgh Liver Research Center, University of Pittsburgh, Pittsburgh, PA; [5]Basic Sciences Division, Fred Hutchinson Cancer Research Center, Seattle, WA 98109; [6]Department of Pathology, Cincinnati Children's Hospital, Cincinnati, OH, 45229; [7]Department of Laboratory Medicine and Pathology, The Mayo Clinic, Rochester, MN, 55905; [8]The UPMC Hillman Comprehensive Cancer Center; [9]The Dept. of Microbiology and Molecular Genetics, The University of Pittsburgh Medical Center, Pittsburgh PA 15224.

Grant Support:

This work was supported by NIH RO1 grants DK103645 to A.W.D., CA174713 to E.V.P. and NCI grant R35 CA231989 to R.N.E and P.C. E.V.P. was also supported by a Mellon Foundation Grant and a UPMC CHP Research Advisory Committee Seed Award. A.R. and J.F. were supported by The UPMC CHP Summer Research Undergraduate Fellowship Program.

Correspondence:

Edward V. Prochownik

Children's Hospital of Pittsburgh

Division of Hematology/Oncology

Rangos Research Center, Room 5124

4401 Penn Ave.

Pittsburgh, PA 15224

Tel: 412-692-6795

Email: procev@chp.edu

Disclosures: The authors declare no potential conflicts of interest.

Preprint server: https://doi.org/10.1101/2021.08.05.455215

Transcript Profiling:

Gene Expres.sion Omnibus(GEO) (Accession number GSE181371(reviewer token: **yvarsegmzpsdbun**), GSE130178 and GSE114634).

Word count: 4258

Author Contributions:

Experimental design: E.V.P, H.W., A.D.

Generation of mouse strains: P.C., R.N.E., H.W.

Hepatocyte transplantation: F.A., A.D.

Histopatholgy studies: M.T., S.R.

Biochemical studies: J.L., A.R., J.F.

RNAseq analyses: H.W.

Manuscript and figure preparation: E.V.P., H.W.

Synopsis

The Myc and Mlx Networks exhibit extensive cross-talk and regulate distinct but overlapping sets of transcriptional targets. The current work demonstrates the cooperation between these two Networks in supporting the regenerative capabilities of normal hepatocytes while also revealing that the Mlx Network serves as a suppressor of spontaneous hepatic adenomatosis.

.

Abstract

Background & Aims. The c-Myc (Myc) bHLH-ZIP transcription factor is deregulated in most cancers. In association with Max, Myc controls target genes that supervise metabolism, ribosome biogenesis, translation and proliferation. This “Myc Network” cross-talks with the “Mlx Network”, which consists of the Myc-like proteins MondoA and ChREBP and Max-like Mlx. Together, this “Extended Myc Network” regulates both common and distinct genes targets. Here we studied the consequence of *Myc* and/or *Mlx* ablation in the liver, particularly those pertaining to hepatocyte proliferation, metabolism and spontaneous tumorigenesis.

Methods. We examined the ability of hepatocytes lacking *Mlx* (*Mlx*KO) or *Myc*+*Mlx* (double KO or DKO) to repopulate the liver over an extended period of time in a murine model of Type I tyrosinemia. We also compared this and other relevant behaviors, phenotypes and transcriptomes of the livers to those from previously characterized *Myc*KO, *Chrebp*KO and *Myc*KO x *Chrebp*KO mice.

Results. Hepatocyte regenerative potential deteriorated as the Extended Myc Network was progressively dismantled. Genes and pathways dysregulated in *Mlx*KO and DKO hepatocytes included those pertaining to translation, mitochondrial function and non-alcoholic fatty liver disease (NAFLD). The Myc and Mlx Networks were shown to cross-talk, with the latter playing a disproportionate role in target gene regulation. All cohorts also developed NAFLD and molecular evidence of early steatohepatitis. Finally, *Mlx*KO and DKO mice displayed extensive hepatic adenomatosis.

Conclusions. In addition to demonstrating cooperation between the Myc and Mlx Networks, this study revealed the latter to be more important in maintaining proliferative, metabolic and translational homeostasis, while concurrently serving as a suppressor of benign tumorigenesis.

Key words: Adenoma, β-catenin, ChREBP, hepatoblastoma, hepatocellular carcinoma, Hippo, MondoA, NAFLD

Introduction

c-Myc (Myc) is a bHLH-Zip transcription factor that regulates numerous target genes, which collectively support survival, proliferation, metabolism, ribosome biogenesis and translation [1-8] . Positive regulation involves Myc's direct sequence-specific DNA binding in heterodimeric association with its obligate bHLH-Zip partner, Max [6, 7]. This occurs at canonical "E-box" elements that typically reside in the vicinity of proximal promoters [9-12]. Bound Myc-Max heterodimers recruit an assortment of transcription co-factors and chromatin modifiers such as histone acetylases and methyltransferases that collectively increase chromatin accessibility, relieve transcriptional pausing and increase the rate and efficiency of mRNA elongation [13-17]. Down-regulation of these genes, often occurring during cellular quiescence or differentiation, involves a reduction in Myc levels and a shift to E-box occupancy by heterodimers now comprised of Max and members of the transcriptionally repressive bHLH-ZIP "Mxd family" that includes Mxd1-4 and the less related Mnt and Mga factors [3, 18-20]. Together, their binding reverses the chromatin modifications mediated by Myc-Max binding and restores transcriptional repression. Negative regulation by Myc is more indirect and involves interaction with and inhibition of positively-acting transcription factors such as Miz1 and Sp1 [21, 22]. The loss of transcriptional balance maintained by these different competing interactions is a feature of transformed cells, which often deregulate and/or over-express Myc [4, 10, 14, 23].

The "Myc Network" cross-talks and shares considerable regulatory overlap with a structurally related but distinct group of bHLH-Zip transcription factors that comprise the so-called "Mlx Network" [1-3, 8, 24, 25][20]. Classically believed to control target gene sets smaller and more functionally restricted than those overseen by Myc, the Myc-like equivalents of the Mlx Network include the transcription factors ChREBP and MondoA. Upon binding glucose and other

nutrients, these cytoplasmic proteins translocate to the nucleus, heterodimerize with the Max-like protein Mlx and bind to their target genes at “carbohydrate response elements” (ChoREs) comprised of tandem E-boxes separated by 5-6 nucleotides [26, 27]. Myc Network and Mlx Network members (collectively termed the “Extended Myc Network”) can bind to one another’s DNA target sequences and some genes are dually regulated by both sets of factors; however the numbers of these genes and the degree to which their regultation is a result of binding to shared versus separate sites has not been clearly delineated [28-32]. Although the Mlx Network is less widely implicated in tumorigenesis than the Myc Network, recurrent *MLX* gene deletions nevertheless occur in as many as 10-20% of several human cancers, with the precise fraction correlating with the size of the deletion (https://portal.gdc.cancer.gov/genes/ENSG00000108788) [1-3, 13, 33][20].

We previously explored the roles for these two networks in normal hepatocyte proliferation utilizing mice lacking the enzyme fumarylacetoacetate hydrolase (FAH). These animals serve as a model for Type I hereditary tyrosinemia in which FAH’s absence allows toxic tyrosine catabolites to accumulate, leading to hepatic necrosis and liver failure [34-36]. Treatment with the drug 2-[2-nitro-4-trifluoromethylbenzoyl]-1,3-cyclohexanedione (NTBC) blocks the enzyme 4-hydroxyphenylpyruvic dioxygenase, which catalyzes the second step in tyrosine catabolism, thus preventing the accumulation of these deleterious intermediates and circumventing the lethal consequences of FAH deficiency. Immuno-compromised FRG-NOD ($Fah^{-/-}$) mice can thus be used as a robust and sensitive animal model in which to evaluate the regenerative potential of any other hepatocyte population, so long as it is *Fah*+/+. Cells are delivered intrasplenically followed by the cyclic withdrawal and reinstatement of NTBC over several months. As recipient hepatocytes accumulate toxic tyrosine intermediates and die, they are replaced by the donor cells, which expand as much as 50-100-fold before eventually comprising up to 70% of the hepatic mass and allowing the recipients to achieve NTBC-independence [25, 37]. The FAH model thus places greater proliferative demands on regenerating hepatocytes than does two-thirds partial

hepatectomy (PH), which represents the gold standard for liver regeneration [38]. It also permits the simultaneous delivery of two or more competing populations of hepatocytes to the same recipient, thus allowing for a direct comparison of their relative proliferative rates within the identical environment.

Using this approach, we previously showed that wild-type (WT) and *Myc-/-* (*Myc*KO) hepatocytes possess indistinguishable regenerative potential [37]. This is quite different from most other cases where Myc's loss in either non-transformed or transformed cells or tissues profoundly suppresses proliferation [25, 37, 39-43]. In contrast, the proliferation of *Chrebp-/-* (*Chrebp*KO) hepatocytes has been show to be significantly impaired and *Myc*KO x *Chrebp*KO hepatocytes are even more defective [25]. These findings indicated that normal hepatocyte regeneration is more dependent upon the Mlx Network than the Myc Network and that the two pathways cross-talk and rescue one another's defects to varying degrees. At the same time, they raise questions about the possible functional redundancy of MondoA in the context of ChREBP's loss.

We have now further explored the relationship between the Myc and Mlx Networks by generating two additional mouse strains. In the first (hereafter referred to as "*Mlx*KO"), deletion of the *Mlx* gene functionally inactivates the entire Mlx Network, including any potential rescue by MondoA that might have existed in *Chrebp*KO mice [25]. The second mouse strain contains a "double knockout" of both *Myc* and *Mlx* (hereafter "DKO") that further inactivates the Extended Myc Network. We show that hepatocytes from both strains, but particularly the latter, are profoundly compromised in repopulating the livers of *Fah-/-* recipients. They also show markedly attenuated expression of genes that are direct targets for both the Myc and Mlx Networks and that control mitochondrial structure and function, ribosomal biogenesis and more general aspects of mRNA processing and translation. Older mice of both groups also develop nonalcoholic fatty liver disease (NAFLD) akin to that previously described in *Myc*KO, *Chrebp*KO or *Myc*KO x

*Chrebp*KO mice. Finally and unexpectedly, over one-third of older *Mlx*KO and DKO mice develop multi-focal hepatic adenomas occasionally associated with small regions of hepatocellular carcinoma (HCC). These results further support the idea that the Myc and Mlx Networks cross-talk and cooperatively regulate a range of pathways related to energy metabolism, lipid balance, translation and proliferation. Finally, they reveal a heretofore unsuspected role for the Mlx Network as a suppressor of benign hepatic adenomatosis [44].

Results

Repopulation by MlxKO and DKO hepatocytes is severely compromised. Donor mouse strains employed for competitive hepatocyte repopulation studies carried homozygous "floxed" alleles of the *Mlx* and/or *Myc* genes (Fig. 1A & B and Table 1) and expressed an albumin promoter-driven Tamoxifen-inducible CreER [25, 45]. Five daily i.p. injections of Tamoxifen were sufficient to allow inactivation of each allele by the time hepatocytes were transplanted 3-4 months later (Fig. 1C).

Using FRG-NOD mice as recipients, we previously showed that WT donor hepatocytes outcompeted an equal number of *Chrebp*KO hepatocytes whereas WT and *Myc*KO hepatocytes competed equally [25, 35, 37]. Suspecting that *Mlx*KO hepatocytes would be even more defective, and to emphasize this, we delivered a total of $3x10^5$ donor hepatocytes intra-splenically into recipient mice at a ~1:6 WT:*Mlx*KO ratio (Fig. 2A & B). After 24-28 wk of NTBC cycling, a number of recipients had died and no survivors had achieved NTBC independence, possibly as a result of the deliberate under-representation of WT hepatocytes in the initial inoculum. Indeed, quantification of the total donor population in the surviving recipients indicated that it comprised only 2-46% of all hepatocytes, which is both lower and more variable than typically achieved when mice receive larger numbers of replication-competent donor cells (Fig. 2C) [25, 37]. Despite this low level reconstitution, the surviving donor hepatocytes were nearly all WT despite their initial minority status ($P<0.001$) (Fig. 2D).

Although *Myc* deletion alone does not confer a replicative disadvantage to hepatocytes, *Chrebp* deletion does and is further exacerbated by the concurrent inactivation of *Myc* [25]. This suggests that the Myc and Mlx Networks are redundant and compensate for one another under certain circumstances. Because *Myc*KO x *Chrebp*KO hepatocytes still express MondoA [25], we asked whether its redundancy might mask more prominent phenotypes. We therefore compared the replicative potential of a mixed population of WT and DKO hepatocytes (1:10 ratio) in which the latter cells have functionally inactivated both ChREBP and MondoA as a consequence of *Mlx* deletion. This experiment achieved a somewhat greater rate of transplant success, with more animals surviving and with recipient livers eventually containing >50% donor hepatocytes (Fig. 2E). As before, however, virtually all these were of WT origin (P<0.001) (Fig. 2F).

To determine more directly which KO population was more proliferatively challenged, an additional competitive transplant experiment was performed using a 1:1 input ratio of *Mlx*KO and DKO donor hepatocytes. Overall survival was again low, no animals achieved NTBC-independence and <2% of hepatocytes isolated from recipients were of donor origin (Fig. 2G). However, despite their own inherent replicative compromise, *Mlx*KO hepatocytes showed an overwhelming survival advantage (Fig. 2H) and comprised nearly 95% of the recovered donor population (P<0.001). Together, these results argue that, in a highly demanding, long-term model of liver regeneration [25, 37, 46, 47], *Mlx* loss and the ensuing functional inactivation of ChREBP and MondoA markedly compromise donor hepatocyte proliferation and/or survival with the additional loss of *Myc* strongly reinforcing the defect.

Overlapping transcriptional dysregulation in MlxKO and DKO livers primarily involves genes with roles in mitochondrial structure and function and translation. Prior to comparing whole transcriptome profiles of WT, *Mlx*KO and DKO livers, we confirmed that the latter two evidenced the predicted dysregulation of their direct target genes. For this, gene set enrichment analysis (GSEA) [48] was performed on three collections of direct Myc target genes from the Molecular

Signatures Data Base C2 collection (MSigDB) (http://www.gsea-msigdb.org/gsea/msigdb/collections.jsp) and a 154 member panel of MondoA/ChREBP/Mlx direct target genes from the Qiagen Ingenuity Pathway Analysis (IPA) Data set (Table 2). In the first case, two of the three Myc target gene sets were also significantly enriched in *Mlx*KO liver RNA seq profiles, indicating as previously shown that some Myc-regulated genes are also responsive to Mlx Network inactivation (Fig. 3A) [13, 24, 25]. That the enrichment of these transcripts was broader and more pronounced in DKO livers, indicated that the Myc Network further contributes to the Mlx Network-mediated regulation of these targets as expected. In the second case, MondoA/ChREBP/Mlx target genes were significantly enriched in both *Mlx*KO and DKO livers (Fig. 3B). These results confirmed that *Myc* and/or *Mlx* inactivation was associated with both unique and shared responses of each Network's respective target genes.

To assess the effect of progressive dismantling of the Extended Myc Network on target gene sets, volcano plots were used to compare individual gene expression profiles in the above livers and previously described *Myc*KO, *Chrebp*KO and *Myc*KO x *Chrebp*KO livers (GEO Accession numbers GSE114634) [25]. In the latter three cases, <30 differences were identified relative to normal livers from age-matched animals (differential expression $\geq$1.5-fold and $q<0.05$) whereas *Mlx*KO and DKO livers showed up to 60-fold more differences (Fig. 3C). This more pronounced gene dysregulation again suggested that the combined loss of ChREBP and MondoA eliminated all redundant functions from the Mlx Network, thereby allowing a much larger complement of gene expression differences to be revealed. The relatively few differences between *Mlx*KO and DKO expression profiles (Fig. 3D and insert) was consistent with the notion that, at least in the normal, non-proliferating liver, the Mlx Network contributes more to regulating both the direct and indirect targets of both Networks. The differences between the DKO vs. *Mlx*KO groups in Fig. 3D were thus comparable to those between WT and *Myc*KO groups shown in Fig. 3C.

IPA profiling of the differentially expressed transcripts in DKO livers (and by extension *Mlx*KO livers) showed that six of the top seven most affected pathways were those with roles in mRNA translation and its control, energy metabolism and mitochondrial structure and function (Fig. 3E). The seeming exception ("Coronovirus Pathogenesis Pathway") contained numerous ribosomal protein transcripts whose dysregulation accounted for this pathway's inclusion. Collectively, these findings agreed with previous reports in livers, liver cancers and other cell types showing the Extended Myc Pathway's role in the above processes [1, 2, 13, 17, 18, 24, 25, 37, 47, 49-52]. Gene expression profiles compiled from the pathways shown in Fig. 3E revealed the down-regulation of numerous transcripts encoding proteins involved in translation and mitochondrial structure and function in *Myc*KO and *Mlx*KO livers and an even greater degree of down-regulation in DKO livers (Fig. 3F&G) [25]).

To explore the potential co-regulation of direct target genes by the Myc and Mlx Networks, we obtained data from the most current version of the Encyclopedia of DNA Elements data base (ENCODE: https://www.encodeproject.org/) [53] and focused on the HepG2 HCC cell line, which was deemed the most relevant to the current work. CRISPR editing had inserted in-frame 3xFLAG epitope tags into the 3'-end of the endogenous *MYC* or *MLX* coding regions, thus allowing all ChIP-seq studies to be performed under identical conditions with the same anti-FLAG antibody. The results were trimmed using a default setting that enumerated only those binding sites within +/-2.5 kb of the transcriptional start site of each gene, thereby maximizing the likelihood of functional relevance. In this way, we identified 4152 genes that bound only Myc, 748 that bound only Mlx and 2433 that bound both factors at 6047 sites, 5267 of which overlapped, either entirely or partially (Fig. 3H). 37% of Myc target genes (2433/6558) also bound Mlx whereas 76% of Mlx target genes (2433/3181) also bound Myc, thus indicating that Mlx target genes are twice as likely to also bind Myc. 50% of the Myc and Mlx binding site peaks mapped to within 65 bp of one another and 75% mapped to within 170 bp, thus indicating that the two factors either bound to the

same E-box or ChoRE or to more than one element in such close proximity that their individual peaks could not be resolved simply by examining the ChIP-seq footprints (Fig. 3I).

To confirm the above results and obtain greater resolution and characterization of Myc and Mlx binding, we analyzed the sequences flanking the sites of maximum factor binding (i.e. the ChiPseq binding "peaks"). The above 6047 binding sites were merged to 2863 distinct sites for motif analysis. 1220 of these (42.6%) contained consensus E-boxes for Myc-Max and 714 contained consensus ChoREs [54](Fig. 3J). 45.2% of the sites contained neither E-boxes nor ChoREs, despite the presence of prominent Myc and/or Mlx footprints, thereby indicating either that the motifs did not conform to the conservative consensus sequences used in our search or that Myc and Mlx binding was indirect as a result of association with other DNA-binding factors.

Remarkably, the E-boxes and ChoREs depicted in Fig. 3J displayed a non-random distribution and tended to occurr within close proximity of factor-binding peaks. The consensus binding sites located closest to or at the peak centers tended to be those whose adjacent sequences contained either the fewest numbers of additional motifs or tightly clustered ones.. This suggested that many ChIP-seq peaks represent the integrated signal of multiple variably overlapping and unresolvable individual binding sites and thus do not necessarily directly overlie a particular site. Collectively, these findings confirm the presence of multiple E-boxes and/or ChoREs within the majority of common target genes as well as direct evidence of Myc's binding to ChoREs and Mlx's binding to E-boxes in select cases. They further suggest a means by which the apposition of multiple binding sites within some genes could allow for the simultaneous binding of different combinations of factors as well as their direct interaction and cross-talk.

Cataloging the functions of the 2433 common genes shown in Fig. 3H using the IPA and Mitoproteome data bases and a bespoke collection of previously published genes [25, 49, 55, 56] showed that many could be categorized as supporting mitochondrial and ribosomal structure and function (Fig. 3K) [25, 55]. Thus, the common Myc- and Mlx-bound target genes in human HepG2

cells faithfully reflect the both the current transcript changes and those previously documented in *Myc*KO and/or *Chreb*KO murine livers and hepatoblastomas [25, 55]. Interestingly, the 4152 genes bound only by Myc and the 748 genes bound only by Mlx fell into somewhat different IPA categories than did the common genes (Fig. 3K). For example, Myc-specific genes were also involved in more restricted and/or unique functions such as TGF-β signaling, cell cycle and oxidative phosphorylation Similarly, Mlx-specific genes also tended to belong to distinct functional categories such as those related to retinoic acid signaling, xenobiotic metabolism, fatty acid β-oxidation and the TCA cycle.

Given the Extended Myc Network's dynamic nature (Fig. 2A), the potential for different members to bind multiple closely neighboring sites with different affinities (Fig. 3J) and their ability to either augment or antagonize one another's transcriptional impact, we hypothesized that Myc and Mlx binding alone (Fig. 3I and J), would not necessarily predict target gene expression levels. We further hypothesized that the transcriptional impact on any individual target gene would ultimately reflect the entire Extended Network's integrated action [57]. We thus examined the expression of the 2433 common Myc and Mlx target genes (Fig. 3H) in 371 human HCCs using data from The Cancer Genome Atlas (TCGA). Target gene expression could be categorized into four groups (designated A-D) that correlated with four patterns of Extended Myc Network member expression (groups 1-4) (Fig. 3L). Two of the tumor groups also showed significant differences in survival (Fig. 3M). Together with the results of Fig. 3J, these findings support the idea that the binding of Myc, Mlx or any other Extended Myc Network factor to a target gene likely reflects only one aspect of the complex and integrative interplay among other Network members that collectively dictates the gene's expression level and downstream biological consequences[20] .

Myc, particularly when it is over-expressed by tumor cells, promotes the Warburg effect by up-regulating glucose transporters and genes encoding glycolytic enzymes [12, 25, 40, 51, 58-63]. However, none of these showed altered expression in *Myc*KO livers (Table 3). However, the

progressive inactivation of the Extended Myc Network was associated with the down-regulation of three transcripts, all of which encode rate-limiting transporters or enzymes. These included the major hepatocyte glucose transporter Glut2/Slc2a2 and the glycolytic enzymes liver-type phosphofructokinase (Pfkl) and liver type pyruvate kinase (Pklr). Glut2/Slc2a2 is also required for the proper regulation of glucose-sensitive genes and for glucose-stimulated insulin secretion [62, 64]. These findings were consistent with the previous IPA showing that genes comprising a glycolysis-related set were co-bound by Myc and Mlx (Fig. 3K).

Loss of the Extended Myc Network members causes NAFLD. Consistent with findings that the Myc and Mlx Networks both impact pathways involved in carbohydrate and lipid metabolism (Fig. 3K) [1, 2, 7, 24, 25, 37, 65, 66], young *Myc*KO, *Chrebp*KO and *Myc*KO x *Chrebp*KO mice develop NAFLD [25, 37, 67]. However, these studies did not determine if this was progressive or if the dual compromise of the Myc and Mlx Networks increased its severity. We therefore examined the livers of older (14-16 month) *Myc*KO, *Chrebp*KO, *Myc*KO x *Chrebp*KO, *Mlx*KO and DKO mice to evaluate the extent of NAFLD. Relative to WT livers, all KO livers showed more intense Oil Red O staining but did not significantly differ from one another (Fig. 4A-F). They also contained more total triglyceride than did livers from younger *Myc*KO, *Chrebp*KO and *Myc*KO x *Chrebp*KO mice [25, 37] (Fig. 4G). These findings suggest that NAFLD appears earlier in *Mlx*KO and DKO mice but that *Myc*KO mice eventually achieve a similar degree of severity.

In further support of the above conclusions, we also found evidence for enrichment of a 163 member gene set associated with human NAFLD in all cohorts except *Chrebp*KO, (https://www.wikipathways.org/instance/WP4396_r98945) (Fig. 4H). Thus, despite the fact that the causes of NAFLD in the above mice and humans differ considerably, there is in most cases considerable similarity in the disease-related gene expression profiles [68].

Finally, we performed IPA to identify additional disease-related pathways that are sometimes dysregulated in NAFLD [68] and in all cases found several relating to lipid

synthesis/metabolism and PPAR activation (Table 4). While noting little histologic evidence for inflammatory cell infiltrates or fibrosis in our KO livers, several of these pathways were in fact associated with non-alcoholic steatohepatitis (NASH) (Table 4). Although these transcriptome-based findings may represent early evidence of actual NASH, the altered expression of inflammatory markers could also be indicative of the immune function changes that accompanies Myc dysregulation in non-hepatic tissues [37, 69]. We believe the most conservative interpretation of the above results is that the NAFLD that accompanies the loss of most Extended Myc Network members exhibits evidence of mild NASH as indicated by significantly altered molecular markers of this state but little documentable histo-pathological change.

MlxKO and DKO mice develop age-related hepatic adenomatosis and occasional HCC. Unexpectedly, 36% of *Mxl*KO and DKO animals (15 of 42) of both genders developed multiple small-medium-sized hepatic neoplasms, which were never observed in WT, *Myc*KO, *Chrebp*KO or *Myc*KO *x Chrebp*KO mice (Fig. 5A&B) [25, 37]. These were mostly well-differentiated and/or myxoid-type tumors with numerous balloon cells, nuclear enlargement and microvesicular steatosis. A minority also showed small foci of well-differentiated HCC, which is sometimes associated with hepatic adenomas in humans (Fig. 5C) [44, 70]. Regardless of histology, adenomas showed significantly more staining for Ki-67 than did the adjacent non-neoplastic liver parenchyma (Fig. 5D, $P=3.4x10^{-5}$).

Adenomas did not express Mlx protein, indicating that they did not originate from residual hepatocytes that had escaped *Mlx* locus excision and maintained their growth advantage (Fig. 5E). Normal livers and DKO adenomas also did not express detectable Myc protein nor did most *Mlx*KO adenomas. This was consistent with their slow growth rates and a likely consequence of their Extended Myc Network defects (Fig. 3C-G) [25, 37]. An exception was seen in a single large adenoma containing elements of HCC from an *Mlx*KO mouse with marked hepatomegaly (liver weight 6.7 g or approx. three times normal) (Fig. 5E).

We performed RNAseq on five adenomas from *Mlx*KO mice and compared their transcriptome profiles to those of WT livers and 45 primary murine hepatoblastomas (HBs) generated by over-expressing the Hippo pathway terminal effector YAP^{S127A} together with one of nine different patient-derived oncogenic mutations of β-catenin [71]. The transcriptional profiles of the adenomas were distinct from those of both livers and all HBs (Fig. 5F&G). Adenomas did not over-express wild-type β-catenin or YAP as is common for HBs [72] but did dysregulate 15 of 22 transcripts that are aberrantly expressed in all murine HBs regardless of etiology and that correlate with survival in human HB and other cancers (Fig. 5H) [47, 73]. Our results indicate that dismantling the Mlx Network, either alone or concurrently with Myc leads to the eventual emergence of multiple adenoma-like hepatic neoplasms (adenomatosis), which, like their human counterparts, can further evolve and acquire HCC-like features [70].

Discussion

Most previous investigations into Myc's role in hepatic regeneration have relied upon the PH model and yielded conflicting results that likely reflected differences in how and when regeneration was assessed and quantified [37]. The short time frame over which this process occurs and the dependency upon separate groups of mice may have further contributed to disparate outcomes. Because post-PH hepatocytes require fewer than two divisions to replace the missing mass, the model also poses a comparatively modest regenerative challenge. Indeed, even this low number overestimates the actual contribution made by dividing hepatocytes given that about half the response to PH involves hypertrophy of the liver remnant plus replicative contributions by non-hepatocyte populations such as endothelial, Kupfer and stellate cells [38, 74, 75]. In contrast, the FAH model is associated with a more sustained and robust 50-100-fold expansion of pure populations of transplanted hepatocytes. It also provides a well-defined point at which a stable level of regeneration can be assessed and a means by which competing donor populations within the same liver can be simultaneously distinguished and quantified following

their delivery at any desired and pre-selected ratio [25, 37, 50]. Using this approach, we previously showed that the long-term proliferation of otherwise normal hepatocytes requires ChREBP but not Myc, although the loss of both factors was additive [25, 37]. Even more pronounced inter-dependencies were seen during HB tumorigenesis, with HB growth being markedly impaired in both *Myc*KO and *Chrebp*KO livers and even more so in *Myc*KO x *Chrebp*KO livers. [25, 46, 47], These findings implied a means of communication between the Myc and Mlx Networks, with each one being able to at least partially rescue defects in the other [1]. They also demonstrated that the requirement for Myc becomes progressively more critical as proliferative demand increases, thus emphasizing it strong contextual dependency (Fig. 6).

Despite our previous transplant studies having been performed with different input ratios of WT and KO hepatocytes [25, 37], their outcomes were consistent with those reported here and allowed us to extend our conclusions regarding the relative importance of the Myc and Mlx Networks in liver regeneration. For example, our studies comparing WT and *Chrebp*KO hepatocytes employed an input inoculum comprised of 62% of the latter population that was reduced by more than half following competitive repopulation [25]. Our current results in which *Mlx*KO hepatocytes comprised ~84% of donor cells but only ~4% of the final population (Fig. 2D) provided strong evidence that the concurrent functional inactivation of both ChREBP and MondoA confers an even more profound proliferative disadvantage. This could be a direct effect resulting from the concurrent loss of ChREBP and MondoA binding to their respective target genes either individually or collaboratively with Myc thereby eliminating any possibility of rescue of one factor by another (Fig. 2A) [24, 26-29]. A non-mutually exclusive indirect effect that allowed Mxd1, Mxd4 and Mnt to suppress Myc target genes more effectively by increasing their association with Max also remains possible (Fig. 2A). The relative importance of these two models could vary among different target genes, at different times during repopulation or in different liver compartments.

We also previously showed that the combined loss of *Myc* and *ChREBP* suppressed regeneration more than did the knockout of either individual gene, thereby corroborating previous evidence for inter-Network cross-talk [2, 3, 13, 24, 25]. In that study, performed with nearly equal contributions of WT and *Myc*KO x *Chrebp*KO donor hepatocytes, the latter was reduced to 7.5% following repopulation [25]. Though markedly impaired, the residual proliferative activity of these cells could have reflected the redundant function of MondoA (Fig. 2A), which is supported by two separate aspects of the current study. The first was the ~45-fold repopulation advantage of WT hepatocytes over DKO hepatocytes, whereas the second was the ~10-fold repopulation advantage of *Mlx*KO hepatocytes over DKO hepatocytes (Fig. 2F&H). Collectively our current results indicate that both the Myc and Mlx Networks play distinct as well as redundant roles in normal hepatocyte replication. However much of the proliferative drive needed to sustain hepatocyte expansion in FAH mice is subsumed by the Mlx Network regardless of the Myc Network's status [25, 37]. This is supported by the progressive deterioration of repopulation potential as the Extended Network is gradually dismantled (Fig. 2C-H) [25].

In proliferatively quiescent cells or organs such as the liver, Myc is usually expressed at low levels and regulates relatively few genes in contrast to Mlx (Figs. 3C and 5E) [25, 37, 76]. Myc's contribution to genome-wide transcription may therefore be better appreciated in tumors where its over-expression can activate genes that are otherwise non-physiologic targets due to their low-affinity binding sites [10, 11, 25, 66]. Another plausible explanation for the seemingly modest transcriptional consequences of Myc loss in some normal tissues is that at least some Myc target gene expression is maintained by the Mlx Network with redundant contributions being made by MondoA and/or ChREBP [25, 37, 76]. This is best appreciated in livers and tumors when the Myc and Mlx Networks are either individually and concurrently inactivated (Fig. 3C) [25].

In tumors, the Myc Network positively regulates most of the genes encoding glycolytic enzymes and strongly contributes to the Warburg effect [5, 12, 40, 49, 51, 59, 63, 77] as it does

in rapidly growing fibroblasts *in vitro* [40, 77]. In contrast, our transcriptomic studies have not revealed such wide-spread roles for the Myc and Mlx Networks in maintaining glycolysis *in vivo* (Table 3 and Fig. 3K), which may reflect Myc's low-level expression, the relative proliferative quiescence of the normal liver and its greater reliance on fatty acid oxidation as an energy source [25, 46, 49, 71]. Nonetheless, among the most down-regulated genes in *Mlx*KO and/or DKO livers, were *Glut2/Slc2a2, Pfkl* and *Pklr* whose encoded proteins are rate-limiting for glucose uptake and glycolysis. In rat insulinoma cells, the *pklr* proximal promoter binds both ChREBP and Myc, with the former interacting with a ChoRE element and the latter binding elsewhere [28, 29]. These results suggest that, in normal liver, glucose uptake and oxidation are more reliant on the Mlx Network (Fig. 6) whereas, in response to Myc-driven transformation or normal proliferation, more extensive transcriptional regulation of glucose uptake and its oxidation is achievable [4, 14, 23, 25, 49, 78]. This could have the additional benefit of maximizing glycolytic efficiency and sustaining cell division when micro-environmental glucose and oxygen supplies were limiting and nutrient-dependent functions of MondoA and ChREBP were attenuated [79].

Coordinated changes in direct and/or functionally-related Myc and Mlx Network target genes were identified in *Mlx*KO and DKO livers but were more pronounced in the latter (Fig. 3A-D) [25, 37]. Some have been previously shown to support protein translation and its control as well as mitochondrial structure and function (Fig. 3E-G) [18, 25, 37, 40, 49, 67, 71]. As was seen for individual glycolysis-related transcripts (Table 3), the collective expression of these sets became increasingly compromised as the Extended Myc Network was progressively inactivated. The dramatic up-regulation of these pathways that accompanies tumorigenesis in WT livers had also been shown to be attenuated in response to Myc and/or ChREBP inactivation and to correlate with slower tumor growth rates [25]. We provided a mechanistic underpinning for the coordinated response of the relevant gene sets associated with these pathways by showing that, in HepG2 cells, 37% of Myc's direct target genes also bind Mlx while 76% of direct Mlx target genes also

bind Myc (Fig. 3H). Many of the previously mapped binding sites for these two factors overlapped and/or contained multiple E-boxes and/or ChoREs (Fig. 3I and J). While this sometimes made it difficult to attribute precisely Myc or Mlx binding to a specific motif within a factor's ChIPseq footprint, the collective binding landscape suggested a model for target gene regulation that accommodated this and all other observations. The model accounted for the fact that many sites containing only E-boxes coincided with Mlx binding peaks whereas many ChoRE-only sites coincided with Myc binding peaks (Fig. 3J). This indicated that cross-talk between the Myc and Mlx Networks occurs by virtue of shared common binding sites as previously suggested. The non-random distribution of E-boxes and ChoREs around Myc and Mlx binding peaks (Fig. 3J) also suggested that more than one such site could be occupied at any given time, that binding might be cooperative and that the composition of the bound factors, their interactions with each other and differential protein-DNA affinities serve to fine tune the target gene's transcriptional output. While we examined only Myc and Mlx binding, these motifs could also bind other Extended Myc Network members such as those between Max and Mxd proteins, which would not have been detected with our ChIPseq analysis. Whether closely-spaced Mlx sites contained ChREBP or MondoA heterodimers could also potentially determine if, when and the degree to which a gene was responsive to metabolic substrate-mediated regulation. Finally, the four groups into which the expression patterns of the 2433 common Myc + Mlx direct target genes in HCCs could be compiled correlated with the patterns of Extended Myc Network transcript expression and, in two cases, with significant survival differences (Fig. 3L and M). In future studies, it will be important to determine the degree to which different neighboring heterodimeric combinations of Extended Myc Network members either cooperate with or antagonize one another under different conditions in different cell types.

Myc and/or ChREBP inhibition are widely associated with lipid accumulation, which stems from an over-reliance on fatty acid oxidation and a resulting increase in lipid uptake that exceeds

the amount necessary to satisfy energy demands (Fig. 4) [25, 37, 65, 80, 81]. Young mice with hepatocyte-specific loss *of Chrebp* or combined *Myc* + *Chrebp* loss also accumulate more neutral lipid than do those with isolated Myc knockout [25]. While we did not serially follow these animals, our findings suggest that, early in life, the partial or complete inactivation of the Mlx Network promotes a more rapid genesis of NAFLD than does inactivation of Myc alone. Over time, however, lipid accumulation equalizes, with little differences among the various KO groups being discernible (Fig. 4G). KO livers dysregulated many of the same gene sets and/or IPA pathways that have been described in NAFLD and its progression in humans (Fig. 4H and Table 4) thereby further supporting the mechanistic relatedness of the various factors responsible for this state. Because KO livers also displayed molecular evidence of incipient NASH, it will be important in future work to determine whether these features become more pronounced with age and whether histological findings of inflammation and fibrosis become discernible [82, 83].

An unanticipated finding was the development of hepatic adenomatosis in more than one-third of *Mlx*KO and DKO mice (Fig. 5A&B). This incidence likely represents an underestimate since animals older than 14-16 mos. were not investigated and microscopic adenomas may have been overlooked in some instances. That similar neoplasms did not appear in WT, *Myc*KO, *Chrebp*KO or *Myc*KO x *Chrebp*KO mice makes it likely that complete Mlx Network inactivation is a pre-requisite for their development. While these neoplasms bear the hallmarks of actual human adenomas [44, 70], several features suggest more aggressive and malignant predilections, despite the lack of Myc expression in most. These include their multi-focality, their occasional HCC-like features and their robust Ki-67 expression (Fig. 5C&D). In contrast, human adenomas, while well-known for their occasional conversion to HCC, are typically few in number and tend to display only modestly higher Ki-67 expression [70]. Molecular features suggestive of more aggressive behavior in our adenomas include the dysregulation of 15 of 22 transcripts that we

recently identified as predicting inferior outcomes in human HBs and over a dozen other human cancer types (Fig. 5H) [47].

Recurrent *MLX* gene deletions are associated with at least eight human cancer types and provide further reason to implicate the Mlx Network in the pathogenesis of hepatic adenomatosis (https://portal.gdc.cancer.gov/genes/ENSG00000108788)[20]. Genetic suppressors of hepatic adenomas and other benign tumors such as meningiomas, neurofibromas and uterine fibroids are well-documented but are distinct from more notorious counterparts such as *TP53, RB, PTEN, APC* and *BRCA1*/2 that are associated with malignant tumors [84-87]. However, the role of Mlx and its members may also be more indirect and nuanced. For example, NAFLD (Fig. 4) is a known predisposing factor for the development of both adenomas and HCC and we are currently unable to determine how it might affect tumorgenesis in *Mlx*KO mice [70, 88, 89]. On the other hand, the failure of *Myc*KO*, Chrebp*KO or *Myc*KO *x Chrebp*KO mice to develop adenomas or HCCs, despite their equally pronounced NAFLD as well as the fact that high-fat diets can actually suppress hepatic tumor growth [90], argues for a more direct role for the Mlx Network in adenoma suppression. It will be of interest to determine whether *Mlx*KO mice are more susceptible to transformation by other oncogenic stimuli even though the emergence of the ensuing tumors may be delayed and their growth slowed.

In summary, we have shown that the Mlx Network engages in considerable biological and molecular cross-talk with the Myc Network and plays a more substantive role in long-term liver regeneration [25, 29, 35, 37, 46]. Both networks, but the former in particular, alter the expression of numerous genes responsible for broad aspects of translation and energy generation by both aerobic and anaerobic pathways [25, 37, 55]. The majority of Myc and Mlx targets are co-regulated or at least bound by both factors, which appear to share many of the same binding sites, which often lie in close proximity to one another. The actual expression of these targets genes further correlates with the patterns of expression of all 13 members of the Extended Myc

Network thereby suggesting complex interactions and inter-dependent cross-talk at their sites of binding. Mechanistically, the defects that ensue in KO cells as a result of compromising these genes reflect an inability to maintain energy production and translation at levels commensurate with their proliferative demands. This is particularly acute in the neoplastic setting where tumor growth, but not induction, may be severely compromised [25, 37, 55]. The presumptive energy dysequilibrium that arises as a consequence of perturbing either or both of the networks is likely addressed by an increased uptake, oxidation and storage of fatty acids leading to eventual NAFLD [25, 71]. The hepatic adenomatosis and occasional HCC seen in response to Mlx Network compromise suggests that the tumor suppressor-like activity of the Mlx Network counters the more pro-oncogenic tendencies of Myc over-expression. Our findings emphasize the elaborate orchestration of the Extended Myc Network in balancing energy demands and metabolism with normal and neoplastic proliferation.

Materials and Methods

Animal studies**.** All breeding, care, husbandry and procedures were approved by The University of Pittsburgh Department of Laboratory and Animal Resources (DLAR) and the Institutional Animal Care and Use Committee (IACUC) with standard animal chow and water provided *ad libitum.* C57BL6 mice expressing GFP (C57BL/6-Tg(UBC-GFP)30Scha, MGI:3057178) have been previously described and were used as a source of wild-type (WT) control hepatocytes due to the ease with which the GFP gene could be identified [25]. C57BL6 *c-myc*$^{LoxP/LoxP}$ mice (B6.129S6-Myc^{tm2Fwa}, MGI:2178233) have been previously described (Fig. 1A) [25, 37, 91, 92] and were obtained as a gift from I. Moreno de Alboran. The generation of mice bearing a 1717 bp deletion spanning exons 3-6 of the *Mlx* locus (*Mlx*KO mice) (Fig. 1B) has also been recently described [8]. Transgenic mice expressing a fusion protein comprised of the hormone-binding domain of the estrogen receptor and Cre recombinase (CreER) and under the control of the albumin promoter that allows CreER to be activated in hepatocytes following tamoxifen exposure

(B6.129S2- Alb$^{tm1(cre/ERT2)Mtz}$, MGI:3052812) were a kind gift of Dr. Frank Gonzalez (Laboratory of Metabolism, Center for Cancer Research National Cancer Institute). The latter mice were bred to homozygosity with *Mlx*$^{LoxP/LoxP}$ mice or *Myc*$^{LoxP/LoxP}$x *Mlx*$^{LoxP/LoxP}$ mice [25, 37]. At weaning, mice were subjected to five daily i.p. injections of tamoxifen (75 mg/Kg each) in corn oil (Sigma-Aldrich, St. Louis, MO). Several weeks later, hepatocytes were harvested as previously described [25, 37]. An aliquot of these was used for DNA isolation and to quantify the extent of *Myc* and/or *Mlx* knockout (Fig. 1). The remainder of the *Myc*KO, *Chrebp*KO or *Myc*KO x *Chrebp*KO hepatocytes were then combined in indicated proportions with WT hepatocytes and a total of $3x10^5$ cells were injected intrasplenically into *Fah-/-* FRG-NOD mice (Yecuris, Inc., Tualatin, OR)[25, 37] (*ChreBP* mice: B6.129S6-Mlxipl^{tm1Ku}, MGI:3043871; *Fah* mice: NOD.Cg-*Rag1*^{tm1Mom} *Fah*^{em1Mvw} *Il2rg*^{tm1Wjl} MGI:5485380). All animals were maintained on 8 mg/L NTBC (Ark Pharm, Libertyville, IL) in their drinking water. After four days, NTBC was discontinued until mice lost approx. 20% of their body weight. NTBC was then re-instated until mice regained their age-appropriate weight. NTBC cycling was continued either until mice had become NTBC-independent (at least 20 wk post-transplantation) or until wk 28 in those cases where NTBC-independence was not achieved. Hepatocyte DNAs were then isolated from recipients and the TaqMan based approaches shown in Table 1 and Fig. 1 were again used to determine the donor:recipient ratio and the relative contribution of each donor population [25, 37]. PCRs were performed in a volume of 12 µl with 50 ng of genomic DNA. Conditions for amplification were 95 °C for 5 min, 40 cycles at 95 °C for 15 s, 60 °C for 60 s.

For gene expression profiling, the above-described *Myc*$^{LoxP/LoxP}$, *Mlx*$^{LoxP/LoP}$ and *Myc*$^{LoxP/LoxP}$x *Mlx*$^{LoxP/LoP}$ mice were bred to B6.129-*Gt(ROSA)26Sor*$^{tm1(cre/ERT2)Tyj}$/J mice (MGI:3699244), which expresses CreER under the control of the ubiquitously-expressed ROSA26 promoter (Jackson Labs) [93]. Excisional inactivation of each locus was initiated at the

time of weaning and confirmed as described above. Liver RNAs were then obtained from mice that were the same age as those used for hepatocyte transplants (~5 mos).

Triglyceride assays. Total lipid was extracted from ~50 mg of liver using the Folch method [94]. Total triglyceride content was then determined as described previously using the Free Triglyceride Reagent (Sigma-Aldrich, Inc.) [25, 95].

Histology, immuno-histochemistry and immuno-blotting. Fresh tissues sections were immediately fixed in formalin, embedded in paraffin and stained with hematoxylin-eosin (H&E) as previously described [25, 37, 49]. Oil Red O (ORO) staining and immuno-histochemistry on snap-frozen sections were also performed as previously described [25, 37]. Tissue samples for immuno-blotting were disrupted in SDS-PAGE lysis buffer containing protease and phosphatase inhibitors but lacking β-mercaptoethanol or Bromophenol Blue as previously described [25, 46, 49, 71]. Protein quantification was performed using the BCA reagent according to the directions of the supplier (Sigma-Aldrich). Following β-mercaptoethanol (1%) and Bromophenol Blue (10%) addition, samples were boiled for 5 min, dispensed into small aliquots and stored at -80C until ready for use. SDS-PAGE and semi-dry transfer to PVDF membranes (Sigma-Aldrich) was performed as previously described [25, 46, 49, 71]. Antibodies used for immuno-blotting included rabbit monoclonals directed against Mlx and Myc (#85570 and #13987, Cell Signaling Technologies, Inc., Danvers, MA) and a mouse monoclonal antibody against GAPDH (#G8795, Sigma-Aldrich). A mouse monoclonal anti-Ki-67 antibody used for immuno-histochemistry was also from Cell Signaling Technologies (#12202). Horseradish peroxidase secondary antibodies were from Santa Cruz Biotechnology (Santa Cruz, CA). Ki-67 immunostain quantification was performed using the ImageJ Immunohistochemistry (IHC) Image Analysis Toolbox (https://imagej.nih.gov/ij/plugins/ihc-toolbox/index.html). All antibodies were used at the dilutions recommended by the suppliers. Immunoblots were developed using an enhanced

chemiluminescent assay kit as directed by the supplier (SuperSignal™ West Pico Plus, Thermo-Fisher, Inc., Waltham, MA).

RNAseq and ChIP-seq experiments. RNAs were purified from five replica tissues of each group of mice using Qiagen RNeasy Mini Kit (Qiagen, Inc. Germantown, MD) followed by DNase digestion [25, 37]. RNA concentration and integrity was confirmed on an Agilent 2100 Bioanalyzer (Agilent Technologies, Foster City, CA) and only those samples with RIN values of >8.5 were used for sequencing. All subsequent analyses were performed as previously described [25, 71]. Sample preparation and sequencing was performed on a NovaSeq 600 instrument (Illumina, Inc., San Diego, CA) by Novagene, Inc. (Sacramento, CA) and raw data were deposited in the National Center for Biotechnology Information (NCBI) Gene Expression Omnibus data base (GEO) (Accession no GSE181371). Data sets from previous RNAseq studies of *Myc*KO, *Chrebp*KO and *Myc*KO x *Chrebp*KO livers and mutant forms of β-catenin+YAP^{S127A} HBs are available from the GEO data base sets GSE114634 and GSE130178 [25, 71]. Differential gene expression was assessed by three different approaches, namely EdgeR, CLC Genomics Workbench version 21 (Qiagen) and DeSeq2, as previously described [25, 47]. When low-abundance reads (cpm <1) were encountered for both comparisons, they were eliminated. Reads from FASTQ files were mapped to the GRCm38.p6 mouse reference genome using STAR (https://github.com/alexdobin/STAR/releases) version 2.7.5. BAM-formatted output was analyzed and transcript abundance was determined by featureCounts (http://bioinf.wehi.edu.au/featureCounts/). Where necessary, Ingenuity Profiling Analysis (IPA) (Qiagen) was used to classify transcripts into pathways whose significance was adjusted for false discovery using the Bonferonni–Hochberg correction. We further utilized Gene Set Enrichment Analysis (GSEA) [48] to identify alterations of functionally-related groups of transcripts from the Molecular Signatures Database (mSigDB) C2 collection (v.7.4) (http://www.gsea-msigdb.org/gsea/msigdb/index.jsp) or from the MitoProteome Data base

(http://www.mitoproteome.org). Volcano plots were generated using the R software package ggplot2 (https://ggplot2.tidyverse.org/) with significant differences between samples being defined as having fold differences >1.5 and false discovery rates <0.05. Heat maps were generated using the ComplexHeatmap package (version 2.6.2, https://bioconductor.org/packages/release/bioc/html/ComplexHeatmap.html). Statistical analyses were performed with R software v4.0.3 (R Foundation for Statistical Computing, Vienna, Austria) and GraphPad Prism v9.00 (GraphPad Software Inc., San Diego, CA).

To analyze ChIP-seq data, we explored the binding Myc and Mlx to their target gene sequences in two different HepG2 cell lines that had been modified using Crispr so as to introduce 3 x FLAG tags at the C-termini of each protein. This allowed ChIP-seq to be performed under identical conditions with a single anti-FLAG antibody. The results were down-loaded from the ENCODE website (https://www.encodeproject.org/) and analyzed using ChIPpeakAnno version 3.13 and the annotation datbase TxDb.Hsapiens. UCSC.hg38.knownGene (R package version 3.13.0.)[96]. Only binding sites residing within +/-2.5 kb of the transcriptional start of each target gene were considered for the current analysis[53, 97]. Overlap between Myc and Mlx binding regions was obtained using the "findOverlapsOfPeaks" funcation (set maxgap = 0, minoverlap = 0). Venn diagrams were used to display unique and overlapping binding sites. FIMO (Version 5.4.1) from the MEME software suite was used to identify E-boxes and ChoREs most closely associated with ChIP-seq peaks. Categorization of genes associated with bound peaks was performed using previous described collections of functionally-related genes or those from the IPA and mitoproteome data bases (Qiagen, Inc. and http://www.mitoproteome.org).

Acknowledgements

Analysis of RNAseq data was supported by The University of Pittsburgh Center for Research Computing. This work was supported by NIH grant RO1 CA174713 and by a Hyundai Hope on Wheels Scholar grant to EVP.

References

[1] Carroll PA, Diolaiti D, McFerrin L, Gu H, Djukovic D, Du J, Cheng PF, Anderson S, Ulrich M, Hurley JB, Raftery D, Ayer DE, Eisenman RN. Deregulated Myc requires MondoA/Mlx for metabolic reprogramming and tumorigenesis. Cancer Cell 2015;27(2):271-85.

[2] Carroll PA, Diolaiti D. A novel role for the extended MYC network in cancer cell survival. Mol Cell Oncol 2016;3(1):e1026528.

[3] Carroll PA, Freie BW, Mathsyaraja H, Eisenman RN. The MYC transcription factor network: balancing metabolism, proliferation and oncogenesis. Front Med 2018;12(4):412-25.

[4] Meyer N, Penn LZ. Reflecting on 25 years with MYC. Nat Rev Cancer 2008;8(12):976-90.

[5] Stine ZE, Walton ZE, Altman BJ, Hsieh AL, Dang CV. MYC, Metabolism, and Cancer. Cancer Discov 2015;5(10):1024-39.

[6] van Riggelen J, Yetil A, Felsher DW. MYC as a regulator of ribosome biogenesis and protein synthesis. Nat Rev Cancer 2010;10(4):301-9.

[7] Wahlstrom T, Henriksson MA. Impact of MYC in regulation of tumor cell metabolism. Biochim Biophys Acta 2015;1849(5):563-9.

[8] Carroll PA, Freie BW, Cheng PF, Kasinathan S, Gu H, Hedrich T, Dowdle JA, Venkataramani V, Ramani V, Wu X, Raftery D, Shendure J, Ayer DE, Muller CH, Eisenman RN. The glucose-sensing transcription factor MLX balances metabolism and stress to suppress apoptosis and maintain spermatogenesis. PLoS Biol 2021;19(10):e3001085.

[9] Kuznetsov VA, Singh O, Jenjaroenpun P. Statistics of protein-DNA binding and the total number of binding sites for a transcription factor in the mammalian genome. BMC Genomics 2010;11 Suppl 1:S12.

[10] Levens D. Cellular MYCro economics: Balancing MYC function with MYC expression. Cold Spring Harb Perspect Med 2013;3(11).

[11] Sabo A, Amati B. Genome recognition by MYC. Cold Spring Harb Perspect Med 2014;4(2).

[12] Dang CV, O'Donnell KA, Zeller KI, Nguyen T, Osthus RC, Li F. The c-Myc target gene network. Semin Cancer Biol 2006;16(4):253-64.

[13] Diolaiti D, McFerrin L, Carroll PA, Eisenman RN. Functional interactions among members of the MAX and MLX transcriptional network during oncogenesis. Biochim Biophys Acta 2015;1849(5):484-500.

[14] Kalkat M, De Melo J, Hickman KA, Lourenco C, Redel C, Resetca D, Tamachi A, Tu WB, Penn LZ. MYC Deregulation in Primary Human Cancers. Genes (Basel) 2017;8(6).

[15] Liu J, Levens D. Making myc. Curr Top Microbiol Immunol 2006;302:1-32.

[16] Tu WB, Shiah YJ, Lourenco C, Mullen PJ, Dingar D, Redel C, Tamachi A, Ba-Alawi W, Aman A, Al-Awar R, Cescon DW, Haibe-Kains B, Arrowsmith CH, Raught B, Boutros PC, Penn LZ. MYC Interacts with the G9a Histone Methyltransferase to Drive Transcriptional Repression and Tumorigenesis. Cancer Cell 2018;34(4):579-95 e8.

[17] Wilde BR, Ayer DE. Interactions between Myc and MondoA transcription factors in metabolism and tumourigenesis. Br J Cancer 2015;113(11):1529-33.

[18] Grandori C, Cowley SM, James LP, Eisenman RN. The Myc/Max/Mad network and the transcriptional control of cell behavior. Annu Rev Cell Dev Biol 2000;16:653-99.

[19] McArthur GA, Laherty CD, Queva C, Hurlin PJ, Loo L, James L, Grandori C, Gallant P, Shiio Y, Hokanson WC, Bush AC, Cheng PF, Lawrence QA, Pulverer B, Koskinen PJ, Foley KP, Ayer DE, Eisenman RN. The Mad protein family links transcriptional repression to cell differentiation. Cold

Spring Harb Symp Quant Biol 1998;63:423-33.
[20] Wang HP, E. . Normal and Neoplastic Growth Suppression by The Extended Myc Network. Preprints 2022.
[21] Gartel AL, Shchors K. Mechanisms of c-myc-mediated transcriptional repression of growth arrest genes. Exp Cell Res 2003;283(1):17-21.
[22] Herkert B, Eilers M. Transcriptional repression: the dark side of myc. Genes Cancer 2010;1(6):580-6.
[23] Nesbit CE, Tersak JM, Prochownik EV. MYC oncogenes and human neoplastic disease. Oncogene 1999;18(19):3004-16.
[24] Billin AN, Ayer DE. The Mlx network: evidence for a parallel Max-like transcriptional network that regulates energy metabolism. Curr Top Microbiol Immunol 2006;302:255-78.
[25] Wang H, Dolezal JM, Kulkarni S, Lu J, Mandel J, Jackson LE, Alencastro F, Duncan AW, Prochownik EV. Myc and ChREBP transcription factors cooperatively regulate normal and neoplastic hepatocyte proliferation in mice. J Biol Chem 2018;293(38):14740-57.
[26] Jeong YS, Kim D, Lee YS, Kim HJ, Han JY, Im SS, Chong HK, Kwon JK, Cho YH, Kim WK, Osborne TF, Horton JD, Jun HS, Ahn YH, Ahn SM, Cha JY. Integrated expression profiling and genome-wide analysis of ChREBP targets reveals the dual role for ChREBP in glucose-regulated gene expression. PLoS One 2011;6(7):e22544.
[27] Poungvarin N, Chang B, Imamura M, Chen J, Moolsuwan K, Sae-Lee C, Li W, Chan L. Genome-Wide Analysis of ChREBP Binding Sites on Male Mouse Liver and White Adipose Chromatin. Endocrinology 2015;156(6):1982-94.
[28] Collier JJ, Zhang P, Pedersen KB, Burke SJ, Haycock JW, Scott DK. c-Myc and ChREBP regulate glucose-mediated expression of the L-type pyruvate kinase gene in INS-1-derived 832/13 cells. Am J Physiol Endocrinol Metab 2007;293(1):E48-56.
[29] Zhang P, Metukuri MR, Bindom SM, Prochownik EV, O'Doherty RM, Scott DK. c-Myc is required for the CHREBP-dependent activation of glucose-responsive genes. Mol Endocrinol 2010;24(6):1274-86.
[30] Billin AN, Eilers AL, Queva C, Ayer DE. Mlx, a novel Max-like BHLHZip protein that interacts with the Max network of transcription factors. J Biol Chem 1999;274(51):36344-50.
[31] Billin AN, Eilers AL, Coulter KL, Logan JS, Ayer DE. MondoA, a novel basic helix-loop-helix-leucine zipper transcriptional activator that constitutes a positive branch of a max-like network. Mol Cell Biol 2000;20(23):8845-54.
[32] Hurlin PJ, Queva C, Eisenman RN. Mnt: a novel Max-interacting protein and Myc antagonist. Curr Top Microbiol Immunol 1997;224:115-21.
[33] Schaub FX, Dhankani V, Berger AC, Trivedi M, Richardson AB, Shaw R, Zhao W, Zhang X, Ventura A, Liu Y, Ayer DE, Hurlin PJ, Cherniack AD, Eisenman RN, Bernard B, Grandori C, Cancer Genome Atlas N. Pan-cancer Alterations of the MYC Oncogene and Its Proximal Network across the Cancer Genome Atlas. Cell Syst 2018;6(3):282-300 e2.
[34] Chinsky JM, Singh R, Ficicioglu C, van Karnebeek CDM, Grompe M, Mitchell G, Waisbren SE, Gucsavas-Calikoglu M, Wasserstein MP, Coakley K, Scott CR. Diagnosis and treatment of tyrosinemia type I: a US and Canadian consensus group review and recommendations. Genet Med 2017;19(12).
[35] Grompe M, Lindstedt S, al-Dhalimy M, Kennaway NG, Papaconstantinou J, Torres-Ramos CA, Ou CN, Finegold M. Pharmacological correction of neonatal lethal hepatic dysfunction in a murine model of hereditary tyrosinaemia type I. Nat Genet 1995;10(4):453-60.
[36] Russo PA, Mitchell GA, Tanguay RM. Tyrosinemia: a review. Pediatr Dev Pathol 2001;4(3):212-21.
[37] Edmunds LR, Otero PA, Sharma L, D'Souza S, Dolezal JM, David S, Lu J, Lamm L, Basantani M,

Zhang P, Sipula IJ, Li L, Zeng X, Ding Y, Ding F, Beck ME, Vockley J, Monga SP, Kershaw EE, O'Doherty RM, Kratz LE, Yates NA, Goetzman EP, Scott D, Duncan AW, Prochownik EV. Abnormal lipid processing but normal long-term repopulation potential of myc-/- hepatocytes. Oncotarget 2016;7(21):30379-95.

[38] Michalopoulos GK. Liver regeneration after partial hepatectomy: critical analysis of mechanistic dilemmas. Am J Pathol 2010;176(1):2-13.

[39] Dubois NC, Adolphe C, Ehninger A, Wang RA, Robertson EJ, Trumpp A. Placental rescue reveals a sole requirement for c-Myc in embryonic erythroblast survival and hematopoietic stem cell function. Development 2008;135(14):2455-65.

[40] Graves JA, Wang Y, Sims-Lucas S, Cherok E, Rothermund K, Branca MF, Elster J, Beer-Stolz D, Van Houten B, Vockley J, Prochownik EV. Mitochondrial structure, function and dynamics are temporally controlled by c-Myc. PLoS One 2012;7(5):e37699.

[41] Landay M, Oster SK, Khosravi F, Grove LE, Yin X, Sedivy J, Penn LZ, Prochownik EV. Promotion of growth and apoptosis in c-myc nullizygous fibroblasts by other members of the myc oncoprotein family. Cell Death Differ 2000;7(8):697-705.

[42] Trumpp A, Refaeli Y, Oskarsson T, Gasser S, Murphy M, Martin GR, Bishop JM. c-Myc regulates mammalian body size by controlling cell number but not cell size. Nature 2001;414(6865):768-73.

[43] Wang H, Mannava S, Grachtchouk V, Zhuang D, Soengas MS, Gudkov AV, Prochownik EV, Nikiforov MA. c-Myc depletion inhibits proliferation of human tumor cells at various stages of the cell cycle. Oncogene 2008;27(13):1905-15.

[44] Donato M, Hamidian Jahromi A, Andrade AI, Kim R, Chaudhery SI, Sangster G. Hepatic adenomatosis: a rare but important liver disease with severe clinical implications. Int Surg 2015;100(5):903-7.

[45] Qu A, Jiang C, Cai Y, Kim JH, Tanaka N, Ward JM, Shah YM, Gonzalez FJ. Role of Myc in hepatocellular proliferation and hepatocarcinogenesis. J Hepatol 2014;60(2):331-8.

[46] Jackson LE, Kulkarni S, Wang H, Lu J, Dolezal JM, Bharathi SS, Ranganathan S, Patel MS, Deshpande R, Alencastro F, Wendell SG, Goetzman ES, Duncan AW, Prochownik EV. Genetic Dissociation of Glycolysis and the TCA Cycle Affects Neither Normal nor Neoplastic Proliferation. Cancer Res 2017;77(21):5795-807.

[47] Wang H, Lu J, Mandel JA, Zhang W, Schwalbe M, Gorka J, Liu Y, Marburger B, Wang J, Ranganathan S, Prochownik EV. Patient-Derived Mutant Forms of NFE2L2/NRF2 Drive Aggressive Murine Hepatoblastomas. Cell Mol Gastroenterol Hepatol 2021;12(1):199-228.

[48] Subramanian A, Tamayo P, Mootha VK, Mukherjee S, Ebert BL, Gillette MA, Paulovich A, Pomeroy SL, Golub TR, Lander ES, Mesirov JP. Gene set enrichment analysis: a knowledge-based approach for interpreting genome-wide expression profiles. Proc Natl Acad Sci U S A 2005;102(43):15545-50.

[49] Dolezal JM, Wang H, Kulkarni S, Jackson L, Lu J, Ranganathan S, Goetzman ES, Bharathi SS, Beezhold K, Byersdorfer CA, Prochownik EV. Sequential adaptive changes in a c-Myc-driven model of hepatocellular carcinoma. J Biol Chem 2017;292(24):10068-86.

[50] Havula E, Hietakangas V. Sugar sensing by ChREBP/Mondo-Mlx-new insight into downstream regulatory networks and integration of nutrient-derived signals. Curr Opin Cell Biol 2018;51:89-96.

[51] Hsieh AL, Walton ZE, Altman BJ, Stine ZE, Dang CV. MYC and metabolism on the path to cancer. Semin Cell Dev Biol 2015;43:11-21.

[52] Li F, Wang Y, Zeller KI, Potter JJ, Wonsey DR, O'Donnell KA, Kim JW, Yustein JT, Lee LA, Dang CV. Myc stimulates nuclearly encoded mitochondrial genes and mitochondrial biogenesis. Mol Cell Biol 2005;25(14):6225-34.

[53] Consortium EP, Moore JE, Purcaro MJ, Pratt HE, Epstein CB, Shoresh N, Adrian J, Kawli T, Davis CA, Dobin A, Kaul R, Halow J, Van Nostrand EL, Freese P, Gorkin DU, Shen Y, He Y, Mackiewicz M, Pauli-Behn F, Williams BA, Mortazavi A, Keller CA, Zhang XO, Elhajjajy SI, Huey J, Dickel DE, Snetkova V, Wei X, Wang X, Rivera-Mulia JC, Rozowsky J, Zhang J, Chhetri SB, Zhang J, Victorsen A, White KP, Visel A, Yeo GW, Burge CB, Lecuyer E, Gilbert DM, Dekker J, Rinn J, Mendenhall EM, Ecker JR, Kellis M, Klein RJ, Noble WS, Kundaje A, Guigo R, Farnham PJ, Cherry JM, Myers RM, Ren B, Graveley BR, Gerstein MB, Pennacchio LA, Snyder MP, Bernstein BE, Wold B, Hardison RC, Gingeras TR, Stamatoyannopoulos JA, Weng Z. Expanded encyclopaedias of DNA elements in the human and mouse genomes. Nature 2020;583(7818):699-710.
[54] Kulakovskiy IV, Vorontsov IE, Yevshin IS, Sharipov RN, Fedorova AD, Rumynskiy EI, Medvedeva YA, Magana-Mora A, Bajic VB, Papatsenko DA, Kolpakov FA, Makeev VJ. HOCOMOCO: towards a complete collection of transcription factor binding models for human and mouse via large-scale ChIP-Seq analysis. Nucleic Acids Res 2018;46(D1):D252-D9.
[55] Wang H, Lu J, Edmunds LR, Kulkarni S, Dolezal J, Tao J, Ranganathan S, Jackson L, Fromherz M, Beer-Stolz D, Uppala R, Bharathi S, Monga SP, Goetzman ES, Prochownik EV. Coordinated Activities of Multiple Myc-dependent and Myc-independent Biosynthetic Pathways in Hepatoblastoma. J Biol Chem 2016;291(51):26241-51.
[56] Cotter D, Guda P, Fahy E, Subramaniam S. MitoProteome: mitochondrial protein sequence database and annotation system. Nucleic Acids Res 2004;32(Database issue):D463-7.
[57] Mandel J, Wang H, Normolle DP, Chen W, Yan Q, Lucas PC, Benos PV, Prochownik EV. Expression patterns of small numbers of transcripts from functionally-related pathways predict survival in multiple cancers. BMC Cancer 2019;19(1):686.
[58] Karim S, Adams DH, Lalor PF. Hepatic expression and cellular distribution of the glucose transporter family. World J Gastroenterol 2012;18(46):6771-81.
[59] Kim JW, Dang CV. Cancer's molecular sweet tooth and the Warburg effect. Cancer Res 2006;66(18):8927-30.
[60] Miller DM, Thomas SD, Islam A, Muench D, Sedoris K. c-Myc and cancer metabolism. Clin Cancer Res 2012;18(20):5546-53.
[61] Osthus RC, Shim H, Kim S, Li Q, Reddy R, Mukherjee M, Xu Y, Wonsey D, Lee LA, Dang CV. Deregulation of glucose transporter 1 and glycolytic gene expression by c-Myc. J Biol Chem 2000;275(29):21797-800.
[62] Thorens B. GLUT2, glucose sensing and glucose homeostasis. Diabetologia 2015;58(2):221-32.
[63] Ward PS, Thompson CB. Metabolic reprogramming: a cancer hallmark even warburg did not anticipate. Cancer Cell 2012;21(3):297-308.
[64] Chadt A, Al-Hasani H. Glucose transporters in adipose tissue, liver, and skeletal muscle in metabolic health and disease. Pflugers Arch 2020;472(9):1273-98.
[65] Muller I, Larsson K, Frenzel A, Oliynyk G, Zirath H, Prochownik EV, Westwood NJ, Henriksson MA. Targeting of the MYCN protein with small molecule c-MYC inhibitors. PLoS One 2014;9(5):e97285.
[66] Soucek L, Evan GI. The ups and downs of Myc biology. Curr Opin Genet Dev 2010;20(1):91-5.
[67] Goetzman ES, Prochownik EV. The Role for Myc in Coordinating Glycolysis, Oxidative Phosphorylation, Glutaminolysis, and Fatty Acid Metabolism in Normal and Neoplastic Tissues. Front Endocrinol (Lausanne) 2018;9:129.
[68] Greco D, Kotronen A, Westerbacka J, Puig O, Arkkila P, Kiviluoto T, Laitinen S, Kolak M, Fisher RM, Hamsten A, Auvinen P, Yki-Jarvinen H. Gene expression in human NAFLD. Am J Physiol Gastrointest Liver Physiol 2008;294(5):G1281-7.
[69] Pello OM, De Pizzol M, Mirolo M, Soucek L, Zammataro L, Amabile A, Doni A, Nebuloni M, Swigart LB, Evan GI, Mantovani A, Locati M. Role of c-MYC in alternative activation of human

macrophages and tumor-associated macrophage biology. Blood 2012;119(2):411-21.
[70] Torbenson M. Hepatic Adenomas: Classification, Controversies, and Consensus. Surg Pathol Clin 2018;11(2):351-66.
[71] Zhang W, Meyfeldt J, Wang H, Kulkarni S, Lu J, Mandel JA, Marburger B, Liu Y, Gorka JE, Ranganathan S, Prochownik EV. beta-Catenin mutations as determinants of hepatoblastoma phenotypes in mice. J Biol Chem 2019;294(46):17524-42.
[72] Sylvester KG, Colnot S. Hippo/YAP, beta-catenin, and the cancer cell: a "menage a trois" in hepatoblastoma. Gastroenterology 2014;147(3):562-5.
[73] Prochownik EV. Reconciling the Biological and Transcriptional Variability of Hepatoblastoma with Its Mutational Uniformity. Cancers (Basel) 2021;13(9).
[74] Itoh T, Miyajima A. Liver regeneration by stem/progenitor cells. Hepatology 2014;59(4):1617-26.
[75] Miyaoka Y, Ebato K, Kato H, Arakawa S, Shimizu S, Miyajima A. Hypertrophy and unconventional cell division of hepatocytes underlie liver regeneration. Curr Biol 2012;22(13):1166-75.
[76] Hofmann JW, Zhao X, De Cecco M, Peterson AL, Pagliaroli L, Manivannan J, Hubbard GB, Ikeno Y, Zhang Y, Feng B, Li X, Serre T, Qi W, Van Remmen H, Miller RA, Bath KG, de Cabo R, Xu H, Neretti N, Sedivy JM. Reduced expression of MYC increases longevity and enhances healthspan. Cell 2015;160(3):477-88.
[77] Wang H, Lu J, Kulkarni S, Zhang W, Gorka JE, Mandel JA, Goetzman ES, Prochownik EV. Metabolic and oncogenic adaptations to pyruvate dehydrogenase inactivation in fibroblasts. J Biol Chem 2019;294(14):5466-86.
[78] Mathsyaraja H, Freie B, Cheng PF, Babaeva E, Catchpole JT, Janssens D, Henikoff S, Eisenman RN. Max deletion destabilizes MYC protein and abrogates Emicro-Myc lymphomagenesis. Genes Dev 2019;33(17-18):1252-64.
[79] Prochownik EV, Wang H. The Metabolic Fates of Pyruvate in Normal and Neoplastic Cells. Cells 2021;10(4).
[80] Zirath H, Frenzel A, Oliynyk G, Segerstrom L, Westermark UK, Larsson K, Munksgaard Persson M, Hultenby K, Lehtio J, Einvik C, Pahlman S, Kogner P, Jakobsson PJ, Henriksson MA. MYC inhibition induces metabolic changes leading to accumulation of lipid droplets in tumor cells. Proc Natl Acad Sci U S A 2013;110(25):10258-63.
[81] Wang H, Sharma L, Lu J, Finch P, Fletcher S, Prochownik EV. Structurally diverse c-Myc inhibitors share a common mechanism of action involving ATP depletion. Oncotarget 2015;6(18):15857-70.
[82] Michelotti GA, Machado MV, Diehl AM. NAFLD, NASH and liver cancer. Nat Rev Gastroenterol Hepatol 2013;10(11):656-65.
[83] Ioannou GN. Epidemiology and risk-stratification of NAFLD-associated HCC. J Hepatol 2021.
[84] Bluteau O, Jeannot E, Bioulac-Sage P, Marques JM, Blanc JF, Bui H, Beaudoin JC, Franco D, Balabaud C, Laurent-Puig P, Zucman-Rossi J. Bi-allelic inactivation of TCF1 in hepatic adenomas. Nat Genet 2002;32(2):312-5.
[85] Lee S, Karas PJ, Hadley CC, Bayley VJ, Khan AB, Jalali A, Sweeney AD, Klisch TJ, Patel AJ. The Role of Merlin/NF2 Loss in Meningioma Biology. Cancers (Basel) 2019;11(11).
[86] Navarro A, Yin P, Monsivais D, Lin SM, Du P, Wei JJ, Bulun SE. Genome-wide DNA methylation indicates silencing of tumor suppressor genes in uterine leiomyoma. PLoS One 2012;7(3):e33284.
[87] Williams EA, Wakimoto H, Shankar GM, Barker FG, 2nd, Brastianos PK, Santagata S, Sokol ES, Pavlick DC, Shah N, Reddy A, Venstrom JM, Alexander BM, Ross JS, Cahill DP, Ramkissoon SH, Juratli TA. Frequent inactivating mutations of the PBAF complex gene PBRM1 in meningioma with papillary features. Acta Neuropathol 2020;140(1):89-93.
[88] Marengo A, Rosso C, Bugianesi E. Liver Cancer: Connections with Obesity, Fatty Liver, and

Cirrhosis. Annu Rev Med 2016;67:103-17.
[89] Brunt EM, Wong VW, Nobili V, Day CP, Sookoian S, Maher JJ, Bugianesi E, Sirlin CB, Neuschwander-Tetri BA, Rinella ME. Nonalcoholic fatty liver disease. Nat Rev Dis Primers 2015;1:15080.
[90] Wang H, Lu J, Dolezal J, Kulkarni S, Zhang W, Chen A, Gorka J, Mandel JA, Prochownik EV. Inhibition of hepatocellular carcinoma by metabolic normalization. PLoS One 2019;14(6):e0218186.
[91] Baena E, Gandarillas A, Vallespinos M, Zanet J, Bachs O, Redondo C, Fabregat I, Martinez AC, de Alboran IM. c-Myc regulates cell size and ploidy but is not essential for postnatal proliferation in liver. Proc Natl Acad Sci U S A 2005;102(20):7286-91.
[92] de Alboran IM, O'Hagan RC, Gartner F, Malynn B, Davidson L, Rickert R, Rajewsky K, DePinho RA, Alt FW. Analysis of C-MYC function in normal cells via conditional gene-targeted mutation. Immunity 2001;14(1):45-55.
[93] Ventura A, Kirsch DG, McLaughlin ME, Tuveson DA, Grimm J, Lintault L, Newman J, Reczek EE, Weissleder R, Jacks T. Restoration of p53 function leads to tumour regression in vivo. Nature 2007;445(7128):661-5.
[94] Folch J, Lees M, Sloane Stanley GH. A simple method for the isolation and purification of total lipides from animal tissues. J Biol Chem 1957;226(1):497-509.
[95] Jouihan H. Measurement of Liver Triglyceride Content. Bio-protocol 2012;2(13):e223.
[96] Zhu LJ, Gazin C, Lawson ND, Pages H, Lin SM, Lapointe DS, Green MR. ChIPpeakAnno: a Bioconductor package to annotate ChIP-seq and ChIP-chip data. BMC Bioinformatics 2010;11:237.
[97] Consortium EP. An integrated encyclopedia of DNA elements in the human genome. Nature 2012;489(7414):57-74.
[98] Mounir M, Lucchetta M, Silva TC, Olsen C, Bontempi G, Chen X, Noushmehr H, Colaprico A, Papaleo E. New functionalities in the TCGAbiolinks package for the study and integration of cancer data from GDC and GTEx. PLoS Comput Biol 2019;15(3):e1006701.
[99] Gu Z, Eils R, Schlesner M. Complex heatmaps reveal patterns and correlations in multidimensional genomic data. Bioinformatics 2016;32(18):2847-9.
[100] Camarda R, Williams J, Goga A. In vivo Reprogramming of Cancer Metabolism by MYC. Front Cell Dev Biol 2017;5:35.

Table 1. qPCR primers and probes used to quantify each of alleles shown in Fig. 1A and B and other necessary genes as indicated.

Name	Sequence of primers and probes	GenBank Acc. No	Location	Target
***Fah* -/-**	FWD: 5′-GGGAGGATTGGGAAGACAATAG-3′	KF947529	4896 -4917	bGH_PA_ terminator
	REV: 5′-ATTCTCCTTGCCTCTGAACATAA-3′	NM_010176	657-635	FAH
	PROBE: 5′ /56-FAM/CTTCTGAGG/ZEN/CGGAAAGAACCAGCT/3IABkFQ/3′	KF947529	4950-4973	bGH_PA_ terminator
GFP	FWD: 5’- AGTGCTTCAGCCGCTACC -3’	MT776902	302-319	eGFP
	REV: 5’- GAAGATGGTGCGCTCCTG -3’	MT776902	393-376	eGFP
	PROBE: 5′/56-FAM/TTCAAGTCC/ZEN/GCCATGCCCGAA/3IABkFQ/-3′	MT776902	346-366	eGFP
***Mlx* WT**	FWD: 5′-TAGCCCAGTGAAGGTCTCA-3′	NC_000077.7	100980807-100980825	Mlx
	REV: 5′-AGGAGTAGACAGGGTAGCTAAT-3′	NC_000077.7	100980911-100980890	Mlx
	PROBE: 5′ /56-FAM/CAGGTCCAG/ZEN/CTTTAGCCCATGTCA/3IABkFQ/3′	NC_000077.7	100980856-100980879	Mlx
***Mlx* - /- (*Mlx*KO)**	FWD: 5′-CACAGGTAGGCAGCAACATA -3′	NC_000077.7	100979147-100979166	Mlx
	REV: 5′-GGAGTGAGGGTGTCTTGTAATC-3′	NC_000077.7	100980990-100980969	Mlx
	PROBE: /56-FAM/CGCCCTTCT/ZEN/ACCCTGTCTACTCCT/3IABkFQ/	N/A	N/A	loxp site
***Myc* WT**	FWD: 5′-GGGAATCCTCACATTCCTACTT-3′	NC_000081.7	61858492-61858513	Myc
	REV: 5′-GATTCAGCACTGGGTGCA-3′	NC_000081.7	61858643-61858626	Myc
	PROBE: 5′ /56-FAM/TAGGAAGAC/ZEN/TGCGGTGAGTCGTGA/3IABkFQ/3′	NC_000081.7	61858549-61858572	Myc
***Myc* -/- (*Myc*KO)**	FWD: 5′-TGATCTGAGCGGTTCCGTA-3′	NC_000081.7	61858570-61858588	Myc
	REV: 5′-TAAAGTCCCAAAGACACTCCAG-3′	NC_000081.7	61863536-61863515	Myc
	PROBE: 5′ /56-FAM/**CCTGCACGA**/ZEN/**TCCGGAACCCTTAAT**/3IABkFQ/3′	NC_000081.7	61858624-61858629	Myc+ loxp site

Table 2. MondoA, ChREBP and Mlx direct target genes from the Qiagen Ingenuity Pathway Analysis Data set.

Symbol	Entrez Gene ID	*Symbol*	Entrez Gene ID	Symbol	Entrez Gene ID	Symbol	Entrez Gene ID
Acaca	107476	*Mrc1*	17533	*Rpl30*	19946	*Rps2*	16898
Acacb	100705	*Mtor*	56717	*Rpl31*	114641	*Rps20*	67427
Acly	104112	*Nr0b1*	11614	*Rpl32*	19951	*Rps21*	66481
Acss2	60525	*Nr1d1*	217166	*Rpl35*	66489	*Rps23*	66475
Adgre1	13733	*Pck1*	18534	*Rpl35a*	57808	*Rps24*	20088
Adipor2	68465	*Pgd*	110208	*Rpl36*	54217	*Rps25*	75617
Agps	228061	*Pklr*	18770	*Rpl36a*	19982	*Rps26*	27370
Anxa2	12306	*Plin1*	103968	*Rpl36al*	66483	*Rps27*	57294
Arntl	11865	*Pnpla2*	66853	*Rpl37*	67281	*Rps27rt*	100043813
Ccl2	20296	*Pnpla3*	116939	*Rpl37a*	19981	*Rps27a*	78294
Ccl7	20306	*Ppara*	19013	*Rpl38*	67671	*Rps27l*	67941
Ccn3	18133	*Pparg*	19016	*Rpl39*	67248	*Rps28*	54127
Cebpa	12606	*Ppargc1a*	19017	*Rpl39l*	68172	*Rps29*	20090
Cidec	14311	*Pygl*	110095	*Rpl3l*	66211	*Rps3*	27050
Cpt1a	12894	*Rgs16*	19734	*Rpl4*	67891	*Rps3a1*	20091
Dhrs7b	216820	*Rpl10*	110954	*Rpl41*	67945	*Rps4y1*	20102
Elovl6	170439	*Rpl10a*	19896	*Rpl5*	100503670	*Rps5*	20103
Fabp4	11770	*Rpl11*	67025	*Rpl6*	19988	*Rps6*	20104
Fasn	14104	*Rpl12*	269261	*Rpl6l*	432502	*Rps7*	20115
Fgf21	56636	*Rpl13*	270106	*Rpl7*	19989	*Rps8*	20116
Foxa1	15375	*Rpl13a*	22121	*Rpl7a*	27176	*Rps9*	76846
Foxa2	15376	*Rpl14*	67115	*Rpl7l1*	66229	*Rpsa*	16785
G6pc	14377	*Rpl15*	66480	*Rpl8*	26961	*Scap*	235623
Gnpat	14712	*Rpl17*	319195	*Rpl9*	20005	*Scd*	20249
Gpam	14732	*Rpl18*	19899	*Rplp0*	11837	*Sirt1*	93759
Gpat3	231510	*Rpl18a*	76808	*Rplp1*	56040	*Slc2a2*	20526
Gpd1	14555	*Rpl19*	19921	*Rplp2*	67186	*Slc2a4*	20528
Hmgcr	15357	*Rpl21*	19933	*Rps10*	67097	*Srebf1*	20787
Hnf1a	21405	*Rpl22*	19934	*Rps11*	27207	*Srsf2*	20382
Hnf4a	15378	*Rpl22l1*	68028	*Rps12*	20042	*Thbs2*	21826
Igf2	16002	*Rpl23*	65019	*Rps13*	68052	*Thrb*	21834
Il1rn	16181	*Rpl23a*	268449	*Rps14*	20044	*Thrsp*	21835
Itgax	16411	*Rpl24*	68193	*Rps15*	20054	*Tkfc*	225913
Khk	16548	*Rpl26*	19941	*Rps15a*	267019	*Tkt*	21881
Lgals3bp	19039	*Rpl27*	19942	*Rps16*	20055	*Txnip*	56338
Lipe	16890	*Rpl27a*	26451	*Rps17*	20068	*Ucp1*	22227
Mlx	21428	*Rpl28*	19943	*Rps18*	20084	*Ucp3*	22229
Mlxip	208104	*Rpl29*	19944	*Rps19*	20085		
Mlxipl	58805	*Rpl3*	27367	*Rps19bp1*	66538		

Table 3. Relative expression levels of transcripts for rate-limiting factors in the glycolytic pathway.

Liver Genotype	Glucose transporter 2 (*Slc2a2*)	Phosphofructokinase-liver type (*Pfkl*)	Pyruvate kinase L/R (*Pklr*)
WT	1.00	1.00	1.00
*Myc*KO	1.19 (q = 1)	0.89 (q = 1)	1.62 (q = 0.66)
*Chrebp*KO	**0.30 (q = 5.0x10^{-5})**	1.07(q = 1)	**0.30(q = 2.0 x10^{-7})**
*Myc*KO x *Chrebp*KO	**0.41(q = 0.02)**	0.95(q = 1)	**0.29(q = 7.0 x 10^{-8})**
*Mlx*KO	**0.10(q = 8.3 x 10 $^{-10}$)**	0.81(q = 0.44)	**0.19(q = 1.0x 10^{-10})**
DKO	**0.13(q = 3.9 x 10^{-9})**	**0.63(q = 0.01**)	**0.16(q = 2.4 x10^{-15})**

Table 4. IPA profiling of KO livers

IPA Diseases & Functions	Cohort	P value
Activation of PPAR in Liver cells	*Myc*KO	< 0.01
	*Chrebp*KO	< 0.01
	*Myc*KO x *Chrebp*KO	< 0.01
	*Mlx*KO	< 0.01
	DKO	< 0.01
Synthesis of Lipids	*Myc*KO	$<10^{-5}$
	*Chrebp*KO	$<10^{-5}$
	*Myc*KO x *Chrebp*KO	$<10^{-5}$
	*Mlx*KO	$<10^{-5}$
	DKO	$<10^{-5}$
Fatty acid metabolism	*Myc*KO	$<10^{-5}$
	*Chrebp*KO	$<10^{-5}$
	*Myc*KO x *Chrebp*KO	$<10^{-5}$
	*Mlx*KO	$<10^{-5}$
	DKO	$<10^{-5}$
Inflammation of liver	*Myc*KO	<0.01
	*Chrebp*KO	<0.01
	*Myc*KO x *Chrebp*KO	<0.01
	*Mlx*KO	<0.01
	DKO	<0.01
Fibrosis of the liver	*Myc*KO	<0.01
	*Chrebp*KO	<0.01
	*Myc*KO x *Chrebp*KO	<0.01
	*Mlx*KO	<0.01
	DKO	<0.01
Hepatic steatosis	*Myc*KO	<0.01
	*Chrebp*KO	<0.01
	*Myc*KO x *Chrebp*KO	<0.01
	*Mlx*KO	<0.01
	DKO	<0.01

Relevant NAFLD-associated IPA pathways in livers from the indicated KO groups compared to WT livers. Because so few gene expression differences existed in *Myc*KO, *Chrebp*KO and *Myc*KO x *Chrebp*KO livers (Fig. 3C), the criteria for differential expression were relaxed to include those genes with >1.2-fold differences and P values <0.05.

Figures

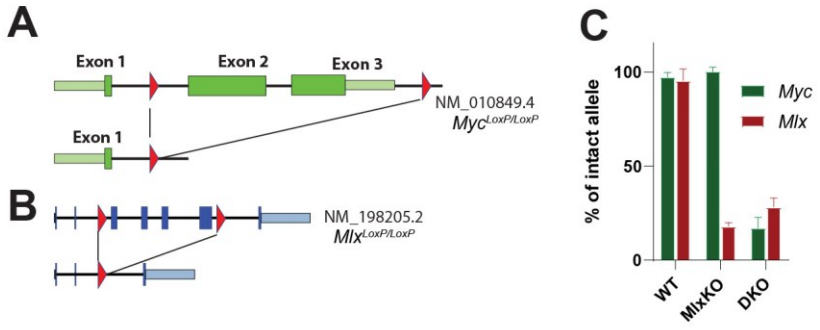

Fig. 1. Strategies for the quantification of total donor and recipient hepatocytes and donor sub-populations. (A). Relevant regions of the murine *Myc* locus prior to and following CreER-mediated recombination showing the location of LoxP sites flanking coding exons 2 and 3 (red triangles) [25, 37]. (B). Relevant regions of the *Mlx* locus prior to and following CreER-mediated recombination showing the location of loxP sites flanking coding exons 3 and 6 [8]. (C) Verification of *MlxKO* and DKO knockouts. 4-5 wks after CreER activation, DNAs from the indicated livers were assessed for the presence of intact or recombined *Myc* and *Mlx* alleles as described in A-C. Hepatocytes were then used for transplant studies. Low-levels of non-excised genes likely originate from the non-hepatocyte populations present in the liver [25, 37].

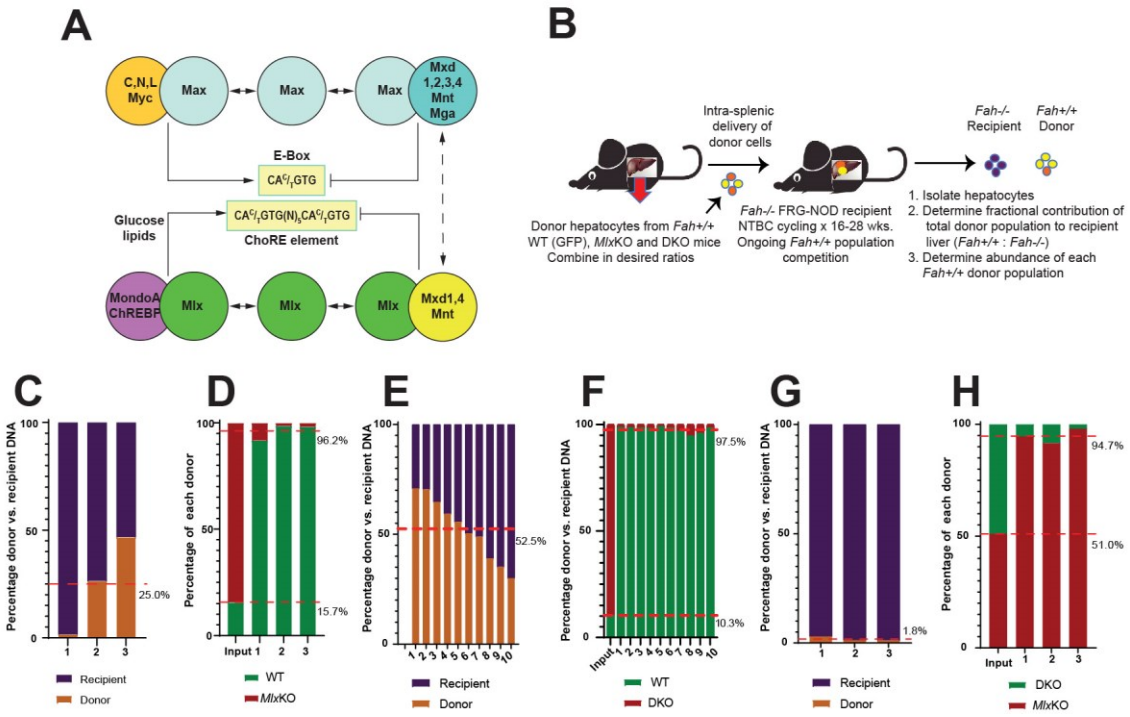

Fig. 2. WT hepatocytes outcompete *Mlx*KO and DKO hepatocytes in repopulation assays. (A). The Extended Myc Network. The top portion of the panel shows the Myc Network, comprised of Myc, Max, Mxd1-4, Mnt and Mga1 and their consensus E-box binding site. The bottom portion shows the Mlx Network and its E-box-related but more complex ChoRE binding site [27, 46]. Mlx interacts with the nutrient-regulated positive factors ChREBP and MondoA or the negative factors Mxd1, Mxd4 and Mnt [2, 13, 24]. The latter cross-talk with the Myc Network (dotted arrow). (B). Hepatocyte transplantation strategy. Isolated *Fah+/+* WT or KO hepatocytes were mixed at the desired ratio and injected intrasplenically into FRG-NOD *Fah*$^{-/-}$ mice maintained continuously on NTBC. NTBC cycling was continued until mice achieved NTBC independence or for 24-28 wks at which time total hepatocytes were isolated and the fractional representation of the total donor and recipient populations determined (Fig. 1). The contribution of each donor set was then further determined and compared to that of the input inoculum. (C). Following intrasplenic injection of $3x10^5$ donor hepatocytes comprised of a 1:6 ratio of WT and *MlxKO* cells, NTBC cycling was

continued for 24-28 wks in the three animals that survived, with none achieving NTBC independence. Hepatocyte DNA was isolated from the transplanted animals and the percentage of recipient and total donor cells was determined**.** (D). DNAs from C were used to determine the ratio of the WT and *MlxKO* donor populations. DNA from an aliquot of hepatocytes at the time of transplant was used to confirm the input donor cell ratio. (E). Transplants performed in FRG-NOD *Fah*$^{-/-}$ mice using inocula containing a ~1:10 ratio of WT:DKO cells. Hepatocytes isolated after 24-28 wks of NTBC cycling showed that, on average, 52.5% of hepatocytes were comprised of donor cells. (F). Hepatocyte DNAs from E were used to determine the fraction of WT and *MlxKO* donor hepatocytes. Lane 1 shows the ~1:10 ratio of the initial input inoculum. (G). Transplants performed in FRG-NOD *Fah*$^{-/-}$ mice using inocula containing a ~1:1 ratio of *MlxKO* and DKO cells. Total hepatocytes isolated after 24-28 wks of NTBC cycling were evaluated for the fractional representation of total donor and recipient populations showing that, on average, <2% of the total hepatocyte mass was of donor origin. (H). Fractional make-up of the donor population from G. Lane 1 shows the ~1:1 ratio of the input population.

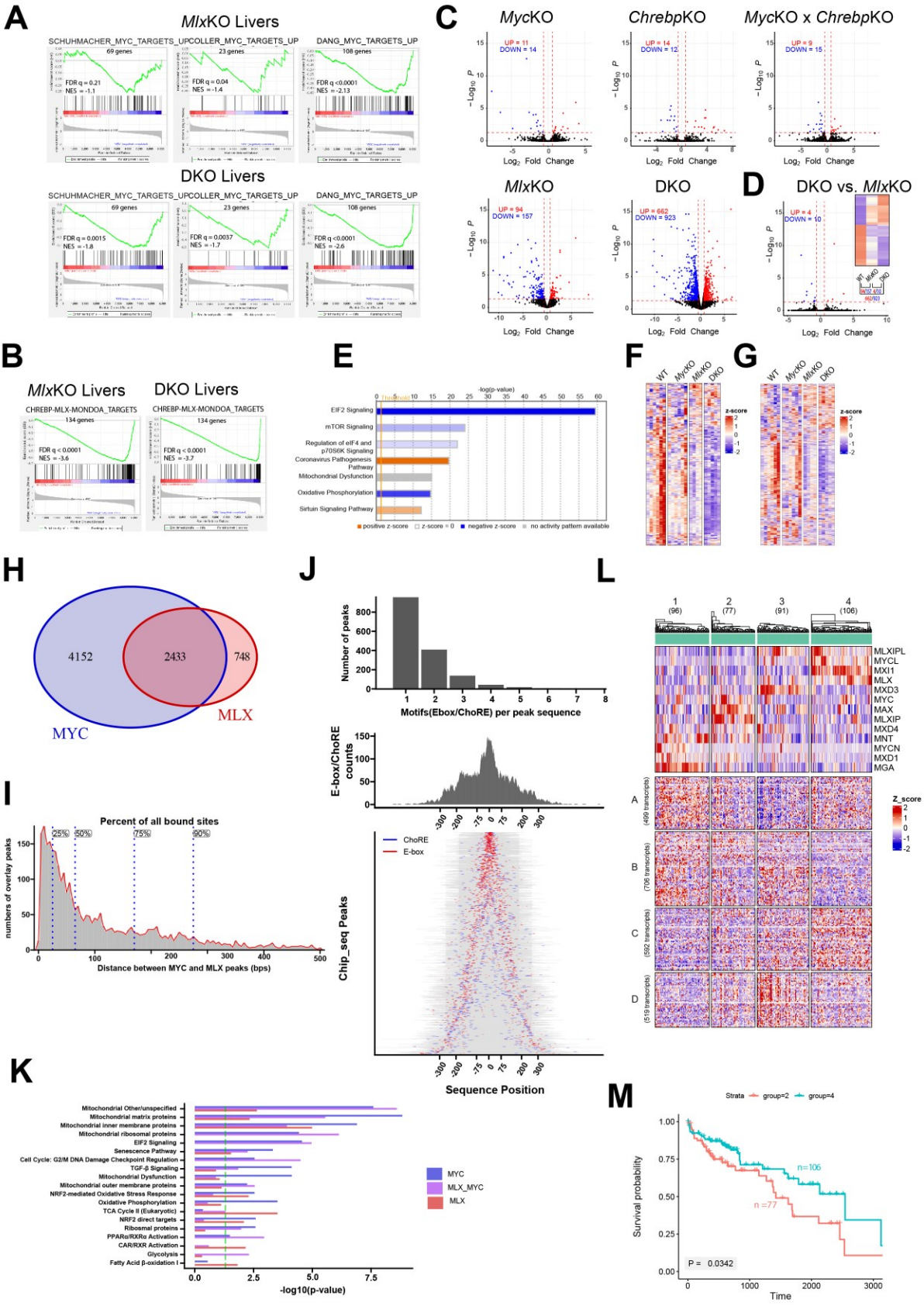
A
MlxKO Livers
SCHUHMACHER_MYC_TARGETS_UP
COLLER_MYC_TARGETS_UP
DANG_MYC_TARGETS_UP
DKO Livers
C
MycKO
ChrebpKO
MycKO x ChrebpKO
MlxKO
DKO
D
DKO vs. MlxKO
B
E
F
G
H
MYC
MLX
4152
2433
748
I
Percent of all bound sites
Distance between MYC and MLX peaks (bps)
J
Number of peaks
Motifs(Ebox/ChoRE) per peak sequence
E-box/ChoRE counts
ChoRE
E-box
Chip_seq Peaks
Sequence Position
L
MLXIPL
MYCL
MXI1
MLX
MXD3
MYC
MAX
MLXIP
MXD4
MNT
MYCN
MXD1
MGA
Z_score
K
MYC
MLX_MYC
MLX
-log10(p-value)
M
Survival probability
Time
P = 0.0342

Fig. 3. Transcriptional dysregulation in response to Myc and/or Mlx Network inactivation. (A). GSEA performed on RNAseq data sets obtained from *MlxKO* and DKO livers. Three sets of direct Myc target genes from the MSigDB Collection containing 69, 23 and 108 members, respectively, were used in the analysis, with expression levels being compared to those of WT livers (N=5 samples per group). (B). A 154 member collection of direct MondoA, ChREBP and Mlx target genes from the Qiagen IPA data set was used in GSEA on the samples shown in A (Table 2). (C). Volcano plots of differentially expressed genes in the indicated livers expressed relative to WT livers. Red and blue points = up-regulated and down-regulated, respectively relative to WT livers. *Chrebp*KO and *Myc*KO x *Chreb*KO liver RNA seq results were obtained from Wang et al. [25]. (D). Comparison of *MlxKO* and DKO livers demonstrating the differential expression of only 14 transcripts. The inset shows a heat map of differentially expressed transcripts among WT, *Mlx*KO and DKO livers. (E). IPA analysis showing the top seven dysregulated pathways in DKO livers. (F). Heat maps of expression differences for 260 transcripts from the MSigDB C2 data base encoding ribosomal subunits and proteins involved in translation (https://www.gsea-msigdb.org/gsea/msigdb/cards/REACTOME_TRANSLATION). (G). Expression differences for 605 transcripts encoding proteins comprising the mitochondrial proteome were compiled from the MitiProteome Data Base (http://www.mitoproteome.org). (H). Myc and Mlx binding sites in HepG2 cells. ChIP-seq results were downloaded from the ENCODE data base (https://www.encodeproject.org/) and analyzed for consensus Myc and Mlx binding sites residing within +/-2.5 kb of transcriptional start sites. The Venn diagram shows genes that bound only Myc, only Mlx or both factors. (I). Proximity of Myc and Mlx binding sites within the common target genes shown in H. Of the 2433 genes shown, a total of 5267 Myc and Mlx binding sites with overlapping footprints were identified. The positions corresponding to the peak center for each factor and the distances between them were determined. (J). The location and identities of E-

boxes and ChoREs in relation to each factor's binding site peaks. Top panel: the number of E-boxes and/or ChoREs associated with each footprint. Middle panel: the proximity of all motifs in relation to their site peak centers (designated as "0"). Bottom panel: The actual location of E-box and ChoRE motifs in each fragment and their position relative to the peak centers. Gray bars correspond to the length (in bps) of sequences that were determined. Some genes are depicted more than once as they contained more than a single non-overlapping binding site. (K). Select functional categories of genes represented by each of the three subsets of genes depicted in (H). Green dotted line: $P < 0.05$. (L). The transcriptomes (HTSeq-FPKM-UQ files) of 371 primary HCCs from TCGA were down-loaded by TCGAbiolinks R package [98] and then assigned to one of four groups (1-4) based on the expression of the indicated members of the Extended Myc Network determined using the ComplexHeatmap R package [99]. Tumors within these groups could be assigned to four additional categories (A-D) based on the expression patterns of the common 2433 transcripts shown in H. 116 of the genes are not shown as their expression was not reported in the TGCA database. (M). Comparative survival of individuals from groups 2 and 4 in (L).

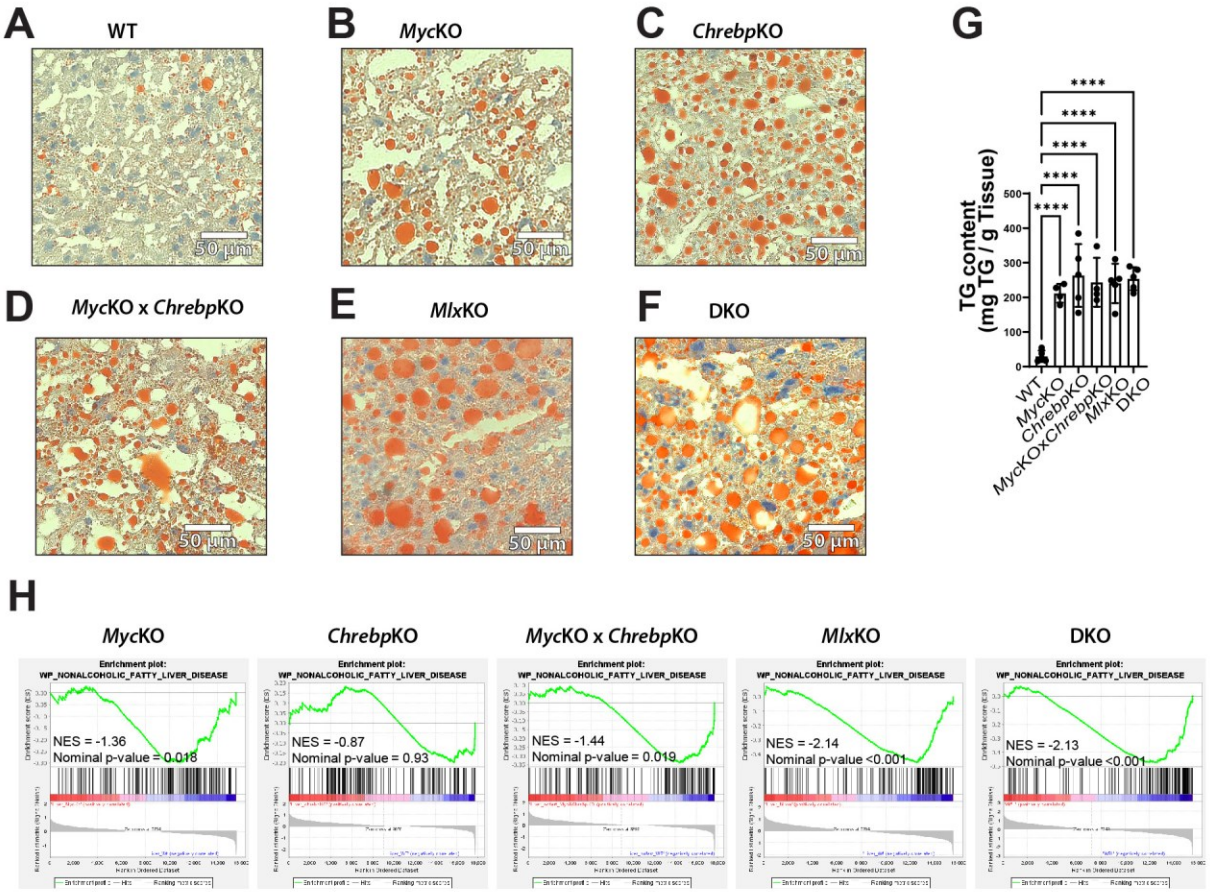

Fig. 4. Neutral lipid accumulation is a feature of livers with compromise of the Extended Myc Network. (A-F). ORO stained sections of livers from 14-16 mo mice of the indicated genotypes. (G). Quantification of triglyceride levels in liver samples from A-F. (H). Enrichment of genes involved in human NAFLD. RNAseq results from the indicated groups of KO mice were compared to their age-matched WT counterparts for the expression of a gene set involved in NAFLD (https://www.wikipathways.org/instance/WP4396_r98945). Normalized enrichment scores (NES) and nominal P values are shown above each profile.

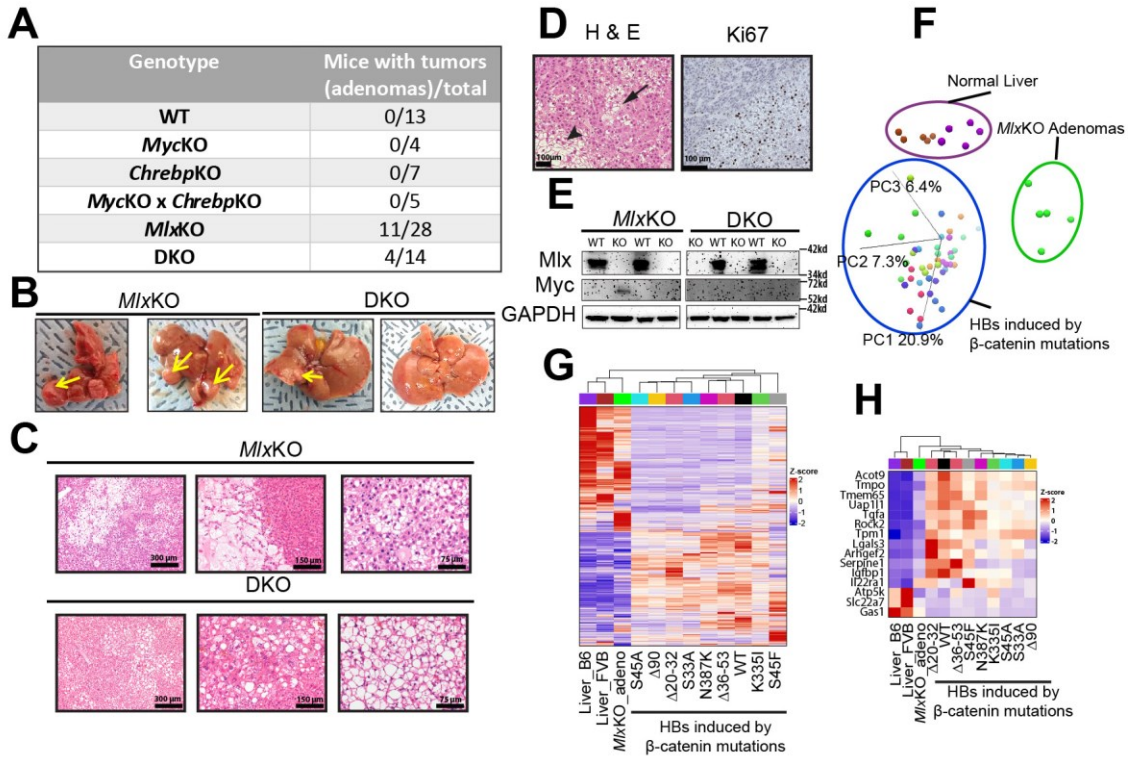

–

Fig. 5. Characterization of hepatic adenomas originating in *MlxKO* and DKO livers. (A). Number of 14-16 mo mice of the indicated genotypes with visible liver tumors at the time of sacrifice. (B). Gross appearance of tumor-containing livers from A. Tumors were generally small but multifocal (arrows). (C). H&E-stained sections showing the typical appearance of *MlxKO* and DKO livers. The first two *MlxKO* images depict well-differentiated and myxoid-type adenomas, respectively, whereas the third panel depicts a focus of well-differentiated HCC embedded within an adenoma. The first two DKO images depict regions of microvesicular steatosis with balloon cells and nuclear enlargement, respectively whereas the third image shows another adenoma that is quite similar in appearance to those arising in *MlxKO* livers. (D). H&E and Ki-67 immuno-stained sections of the Myc-expressing adenoma from D showing regions of inflammation (arrowhead), adjacent to those resembling well-differentiated HCC (arrow). Ki-67 staining is more intense within the nodular adenoma (lower right) compared to adjacent normal liver (upper left). Quantification of Ki-67 staining from four different adenomas and adjacent normal tissue was

performed on 300-2000 cells from each region. The mean Ki-67 index in adenomas was 30.08+/-6.5%% versus 3.2+/-3.1% in adjacent non-adnomatous tissues ($P=3.4x10^{-5}$). (E). Immuno-blots showing Mlx expression in WT livers and its absence in adenomas arising from *MlxKO* and DKO livers. Only one large adenoma from an *MlxKO* mouse with hepatomegaly expressed detectable levels of Myc (lane 2). (F). PCA of whole transcriptomes from WT livers, HBs generated by the over-expression of mutant forms of β-catenin+YAP^{S127A} and the above-described adenomas. (G). Whole transcriptome profiles of the tissues from F. Note that control liver samples are derived from two different strains, C57B6 and FVB. (H). Heat maps of 15 of the 22 transcripts that are dysregulated in murine HBs and correlate with poor outcomes in human HBs and other human cancers [47].

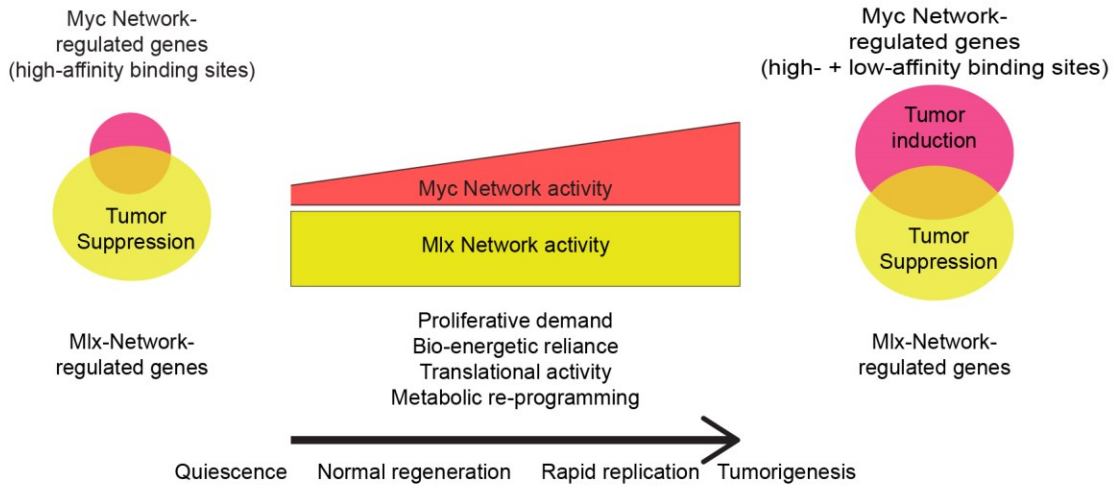

Fig. 6. A model for gene regulation and control of normal and neoplastic proliferation by the Extended Myc Network. During quiescence, Myc levels are low and its target genes, which are relatively few in number (Fig. 3 and [76]) tend to be those with high-affinity E-box binding sites. Slow and controlled replication, such as that occurring during the replacement of *Fah-/-* hepatocytes, is largely regulated via the Mlx Network [25, 37]. As replication increases or as cells acquire transformed features, increased Myc expression [25, 49] activates genes with low-affinity binding sites, including those encoding glycolytic enzymes that are collectively responsible for the Warburg effect as well as other metabolic pathways and functions that support increased energy demands and rapid growth [2, 3, 24, 40, 51, 63, 67, 100]. Despite the rapid growth that occurs in response to the over-expression of Myc and mutant forms of β-catenin and YAP^{S127A} [25, 49, 71] the Mlx Network, which supports this rapid growth, is proposed to also contribute to tumor suppression as well (Fig. 5).